Design, Synthesis, and Biological Evaluation of New Cyclic Disulfide Decapeptides That Inhibit the Binding of AP-1 to DNA

Keiichi Tsuchida,*,† Hisaaki Chaki,‡ Tadakazu Takakura,† Junichi Yokotani,† Yukihiko Aikawa,‡ Shunichi Shiozawa,§,∥ Hiroaki Gouda,⊥ and Shuichi Hirono⊥

Discovery Laboratories and Research Laboratories, Toyama Chemical Co., Ltd., 4-1 Shimookui 2-chome, Toyama 930-8508, Japan, Department of Rheumatology, Faculty of Health Science, Kobe University School of Medicine, 7-10-2 Tomogaoka, Suma-ku, Kobe 654-0142, Japan, Rheumatic Disease Division, Kobe University Hospital, 7-5-2 Kusunoki-cho, Chuo-ku, Kobe 650-0017, Japan, and School of Pharmaceutical Sciences, Kitasato University, 5-9-1 Shirokane, Minato-ku, Tokyo 108-8641, Japan

Received February 4, 2004

The transcription factor activator protein-1 (AP-1) is an attractive target for the treatment of immunoinflammatory diseases, such as rheumatoid arthritis. Using the three-dimensional (3D) X-ray crystallographic structure of the DNA-bound basic region leucine zipper (bZIP) domains of AP-1, new cyclic disulfide decapeptides were designed and synthesized that demonstrated AP-1 inhibitory activities. The most potent inhibition was exhibited by Ac-*c*[Cys-Gly-Gln-Leu-Asp-Leu-Ala-Asp-Gly-Cys]-NH_2 (peptide **2**) (IC_{50} = 8 μM), which was largely due to the side chains of residues 3–6 and 8 of the peptide, as shown by an alanine scan. To provide structural information about the biologically active conformation of peptide **2**, the structures of peptide **2** derived from molecular dynamics simulation of the bZIP–peptide **2** complex with explicit water molecules were superimposed on the solution structures derived from NMR measurements of peptide **2** in water. These showed a strong structural similarity in the backbones of residues 3–7 and enabled the construction of a 3D pharmacophore model of AP-1 binding compounds, based on the chemical and structural features of the amino acid side chains of residues 3–7 in peptide **2**.

Introduction

Activator protein-1 (AP-1) is an important transcription factor for genes involved in immune and inflammatory responses, such as cytokines and collagenase.[1-3] Various inflammatory and mitogenic stimulations lead to AP-1 activation, and it probably plays a role in rheumatoid arthritis, transplant rejection, and tumor growth, so it is an attractive therapeutic target for the treatment of such disorders.[4] Indeed, systematic administration of an AP-1 decoy oligodeoxynucleotide containing the AP-1 binding site was found to inhibit arthritic joint destruction in mice with collagen-induced arthritis.[5] AP-1 is composed of members of the Fos and Jun families.[1] Fos and Jun proteins dimerize through a leucine zipper motif at their carboxyl terminals and bind DNA through a basic region that is located immediately upstream of the leucine zipper.[1,6] The three-dimensional (3D) X-ray crystallographic structure[7] of the basic region leucine zipper (bZIP) domains of c-Fos and c-Jun bound to a 20 nucleotide DNA duplex containing the AP-1 binding site revealed single α-helices and showed that the heterodimer grips the major groove of the DNA like a pair of forceps. Although the solution structure of the bZIP domains of AP-1 in the absence of DNA is unclear, the effect of dimerization and DNA binding on circular dichroism (CD) spectra of the bZIP domains suggested that the basic regions of the domains take on an α-helical conformation only in the presence of DNA.[8] In support of this, the solution structure of the yeast transcriptional factor GCN4 bZIP domain, as determined by NMR, revealed that the leucine zipper region forms a long uninterrupted α-helix and the basic region is flexible but structured, fluctuating around a helical conformation in the absence of DNA.[9]

Structure-based drug design methods have strongly enhanced the lead discovery and optimization process using the 3D structures of target proteins, which are important for understanding the interaction between the ligand and the target protein.[10,11] Recently, natural products such as curcumin,[12,13] dihydroguaiaretic acid,[12,14] momordin,[15] and a new anthraquinone derivative[16] were reported to inhibit the binding of AP-1 to the AP-1 binding site. However, 3D structural information about the AP-1 binding of these inhibitors is not yet available.

We therefore carried out the de novo design of cyclic peptides exhibiting AP-1 inhibitory activity using the 3D structure of the bZIP domains from the X-ray crystal structure of the AP-1–DNA complex.[7] Our aim was to construct a hypothetical 3D pharmacophore model for generating new AP-1 inhibitors. A pharmacophore model is defined as the 3D arrangement of the structural and physicochemical features that are relevant to biological activity and is a versatile tool to aid in the discovery and development of new lead compounds.[17]

Cyclization of a flexible linear peptide is known to reduce the conformational freedom of the peptide and restrict its possible conformations, often resulting in

* To whom correspondence should be addressed. Tel: +81-76-431-8218. Fax: +81-76-431-8208. E-mail: KEIICHI_TUCHIDA@toyama-chemical.co.jp.
† Discovery Laboratories, Toyama Chemical Co., Ltd.
‡ Research Laboratories, Toyama Chemical Co., Ltd.
§ Kobe University School of Medicine.
∥ Kobe University Hospital.
⊥ Kitasato University.

10.1021/jm049890+ CCC: $27.50
Published on Web 07/21/2004

higher receptor binding affinity.[18,19] Several methods for cyclization are known, and we selected the disulfide method, which forms a side chain−side chain disulfide bridge between the N- and the C-terminal Cys residues.

Here, we report the rational design and synthesis of cyclic disulfide decapeptides and their inhibitory activities as evaluated by an AP-1 binding assay. Ac-*c*[Cys-Gly-Gln-Leu-Asp-Leu-Ala-Asp-Gly-Cys]-NH_2 (peptide **2**) exhibited the most potent inhibitory activity (IC_{50} = 8 μM) among these peptides. Furthermore, we built a pharmacophore model based on the chemical and structural features of peptide **2** obtained from an alanine scan and structural studies using a combination of NMR and molecular dynamics (MD) simulations of peptide **2**.

Methods

Molecular Modeling and de Novo Design. The crystallographic coordinates of the bZIP domains of AP-1 were obtained from the Brookhaven Protein Data Bank, entry 1FOS,[7] followed by the addition of hydrogen atoms to the bZIP domains with standard geometry. All molecular modeling and docking studies were performed using the SYBYL software package version 6.4[20] running on a Silicon Graphics Power Indigo2 workstation. All of the peptides used in this study were built using the Biopolymer module. The designed peptides were N-terminal-acetylated and C-terminal-amidated. Ionizable residues in the bZIP domains and designed peptides were assumed to be charged under physiological conditions. Docking was performed with the manual docking module DOCK. Our design was based on the AP-1 DNA binding site topology from the X-ray crystal structure of the AP-1−DNA complex. In the complex, Asn147 and Arg155 of c-Fos and Asn271 of c-Jun interact with the bases of the AP-1 binding site by hydrogen bonds, whereas the β-carbons of Ala150, Ala151 and Ser154 of c-Fos and Ala274, Ala275 and Ser278 of c-Jun come in contact with the 5-methyl groups of thymine bases of the AP-1 binding site by hydrophobic interactions.[7] The residues involved in these interactions are essential for the high-affinity binding of AP-1 to DNA.[21-26] On the basis of these interactions between the bZIP domains and the DNA, the candidate peptides were manually docked in the binding site. In particular, several spatial orientations and conformations of peptides were evaluated in the binding site of the bZIP domains.

Minimization of each complex obtained by docking was performed to reach a final convergence of 0.001 kcal mol^{-1} $Å^{-1}$ by the Powell method in the MAXIMIN2 module of SYBYL. The Tripos force field[27] was used for the energy minimizations, and a dielectric constant of 78.3 was employed. Partial atomic charges were calculated by the method of Gasteiger and Hückel.[28,29] The intermolecular energy of the peptide−binding site interaction was used to evaluate the quality of the docking experiment.

MD Simulations. The MD calculations were performed with AMBER version 4.1.[30] The structure of the bZIP−peptide **1** (Ac-*c*[Cys-Gly-Gln-Leu-Asp-Leu-Ala-Leu-Gly-Cys]-NH_2) complex obtained by docking was covered with an 18 Å shell of 9163 water molecules. The TIP3P model was used as the water model.[31] The resulting structure of the complex was optimized using energy minimization until the root-mean-square (RMS) value of the potential gradient was <0.05 kcal mol^{-1} $Å^{-1}$. MD simulation was then performed for 100 ps at 310 K with a dielectric constant of 1.0. Next, the initial structure of the bZIP−peptide **2** complex was constructed by the replacement of Leu in position 8 of peptide **1** with Asp while maintaining the original side chain orientation in the bZIP−peptide **1** complex after removing water molecules using the Biopolymer module of SYBYL 6.4. The structure obtained was covered with a 22 Å shell of 12 810 water molecules. After energy minimization of the structure, MD simulation was carried out for a period of 400 ps. The model structure obtained after MD simulation was minimized using the conditions described above.

The SHAKE algorithm was employed to restrain the bond lengths in order to remove the high-frequency motions.[32] This allowed us to use a time step of 1 fs. We used the dual nonbonded cutoff method with a primary cutoff of 9 Å and a secondary cutoff of 12 Å. The nonbonded pair list was updated every 20 time steps in the MD calculations. All calculations were carried out using a Silicon Graphics Power Indigo2 workstation.

Results and Discussion

De Novo Design. We designed candidate peptides using a combination of aliphatic hydrophobic amino acids such as Leu, Ile, and Val, acidic amino acids such as Asp and Glu, and neutral polar amino acids such as Asn and Gln. bZIP domains lack a binding cavity, so we chose a manual rather than an automated docking procedure. First, we searched for a tripeptide to interact with the residues, Asn147, Ala150, Ala151, Ser154, and Arg155 in the basic region of c-Fos, which participate in contacts with the bases of the AP-1 binding site of DNA. We chose Ac-Asn-Leu-Asp-NH_2 to assume the hydrogen-bonding interaction between the Asn residue and the Asn147 and between the Asp residue and the Arg155 and the hydrophobic interaction between the Leu residue and the residues, Ala150, Ala151, and Ser154, and then, we docked the tripeptide into the binding site of the bZIP domains (Figure 1a). Next, we elongated the tripeptide stepwise at the C terminus by one residue increments to the hexapeptide Ac-Asn-Leu-Asp-Leu-Ala-Leu-NH_2 to interact with the residues Asn271, Ala274, Ala275, and Ser278 in the basic region of c-Jun. Finally, we built the cyclic disulfide decapeptide Ac-*c*[Cys-Gly-Asn-Leu-Asp-Leu-Ala-Leu-Gly-Cys]-NH_2 by addition of Cys-Gly residues at the N terminus and Gly-Cys residues at the C terminus to the hexapeptide and by cyclization of the resulting decapeptide. On the basis of the docking model of the cyclic peptide, we designed several cyclic peptides by replacement of a residue of the cyclic peptide by appropriate residue to assume an interaction with the putative binding site in the bZIP domains. By way of example, Figure 1b shows the docking model of peptide **1**, obtained by replacement of Asn3 with Gln and energy minimization. After evaluating the quality of the docking experiment by the interaction energy between the designed peptide and the bZIP domains, decapeptides with relatively large interaction energies were synthe-

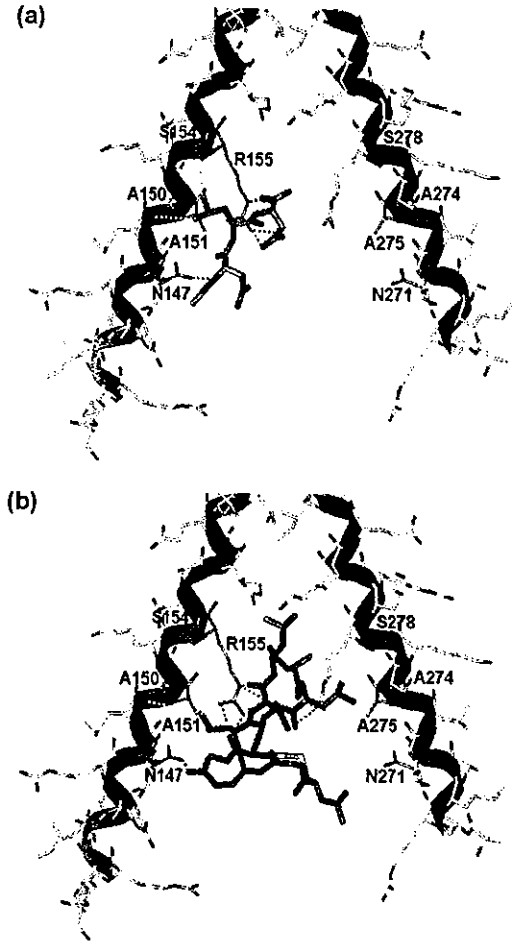

Figure 1. Docking models of the designed peptides with the binding site in the bZIP domains. (a) Ac-Asn-Leu-Asp-NH_2, pink; (b) peptide **1**, green. Ribbon representation of the Fos and Jun basic regions (c-Fos, cyan; c-Jun, magenta). Orange residues, residues involved in AP-1–DNA interactions; red broken lines, putative hydrogen bonds; yellow broken lines, putative hydrophobic interactions.

sized using the standard solid phase methodology with Fmoc chemistry and were evaluated using AP-1 binding assays in which peptides competed for the binding of digoxigenin (DIG)-labeled oligonucleotides containing the AP-1 binding site. Among these peptides, peptide **1** exhibited a weak inhibitory activity at 1 mM, whereas the corresponding linear peptide Ac-Gln-Leu-Asp-Leu-Ala-Leu-NH_2 exhibited no inhibitory activity at same concentration. It was assumed that cyclization of the flexible linear peptide converted it from an inactive to an active conformation.

Next, we performed the MD simulation of the bZIP–peptide **1** complex obtained by docking in order to relax the structure. The resulting structure of the complex from the MD simulation at 100 ps is shown in Figure 2. On the basis of the complex structure after 100 ps, we designed several cyclic peptides to interact more strongly with the putative binding site in the bZIP domains. Replacement of Leu with Asp in position 8 of peptide **1** resulted in Ac-*c*[Cys-Gly-Gln-Leu-Asp-Leu-Ala-Asp-Gly-Cys]-NH_2 (peptide **2**), which was found to possess a more potent inhibitory activity ($IC_{50} = 8\ \mu M$).

We synthesized analogues of peptide **2** in which each Gly was deleted to reduce the ring size and produce more constrained cyclic decapeptides. However, each

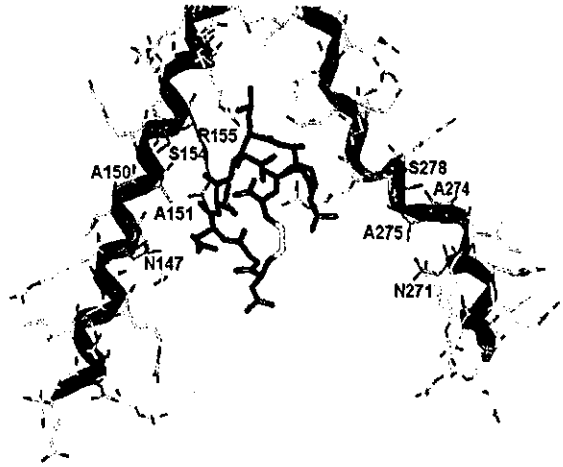

Figure 2. Snapshot taken from MD simulation of the bZIP–peptide **1** complex at 100 ps. The color coding is the same as in Figure 1.

resulting cyclic nonapeptide (Table 1; peptides **3** and **4**) demonstrated a significant loss of inhibitory activity. It was assumed that reduction of the ring size of the peptide backbone altered the peptide from an active to an inactive conformation.

Alanine Scan of Peptide 2. To evaluate the contributions of each of the amino acid side chains, we synthesized analogues of peptide **2** in which each residue, except for Cys, was substituted with Ala (Table 1; peptides **5**–**11**). This strategy has recently been used to identify the amino acid side chains participating in ligand–receptor interactions while preserving the configuration of the peptide backbone and maintaining a similar conformation.[33–36] Substitutions of Leu4, Asp5, Leu6, and Asp8 by Ala resulted in a nearly complete loss of inhibitory activities at 100 or 200 μM. Substitution of Gln3 by Ala resulted in only weak inhibitory activity. Substitution of the aspartic acid side chain in position 5 showed the greatest effect. These results indicate that side chains of Gln3, Leu4, Asp5, Leu6, and Asp8 in peptide **2** contribute significantly to inhibitory activity against the binding of AP-1 to DNA. Peptides **5** and **11**, in which each Gly residue had been substituted by Ala, were devoid of inhibitory activities. It was assumed that replacement of Gly by Ala, which is expected to restrict the conformational freedom of the peptide backbone at this point, changed the active conformation of the peptide to an inactive form.

Modification of Peptide 2. Although an alanine scan is useful for identifying important side chains, such analogues provide little information about the nature of the interactions or indirect effects due to changes in the peptide structure. To examine optimal side chains and obtain a more potent inhibitor, we synthesized analogues in which each side chain in peptide **2** was substituted with a more subtle isosteric or isoelectronic amino acid (Table 1; peptides **12**–**18**).

Gln3 was substituted with Glu or Lys (peptides **12** and **13**), resulting in complete loss of inhibitory activity at 200 μM. Substitution with Asn, causing contraction of the carboxamide side chain (peptide **14**), resulted in a moderate loss of inhibitory activity (>10-fold).

Substitution of Leu with the more hydrophobic amino acid cyclohexylalanine (Cha) (peptides **15** and **16**) resulted in a nearly complete loss of inhibitory activity.

Table 1. Analytical Data and Percentages of Inhibition at 100 μM and IC_{50} of Synthetic Peptides (**2**–**18**) of the Form Ac-c[Cys-A^2-A^3-A^4-A^5-A^6-A^7-A^8-A^9-Cys]-NH_2

peptide	sequence								MS		HPLC t_R (min)[d]		% inhibition	
	A^2	A^3	A^4	A^5	A^6	A^7	A^8	A^9	calcd[a]	obsd[b]	method 1	method 2	at 100 μM	IC_{50} (μM)
2	Gly	Gln	Leu	Asp	Leu	Ala	Asp	Gly	1033.4	1033.8	11.42	8.76	81	8
3		Gln	Leu	Asp	Leu	Ala	Asp	Gly	974.4[c]	974.8[c]	11.06	9.47	−2	>100
4	Gly	Gln	Leu	Asp	Leu	Ala	Asp		974.4[c]	974.8[c]	11.12	9.72	11	>100
5	Ala	Gln	Leu	Asp	Leu	Ala	Asp	Gly	1047.4	1047.3	11.34	9.51	5	>100
6	Gly	Ala	Leu	Asp	Leu	Ala	Asp	Gly	976.4	976.8	12.36	11.10	29	>100
7	Gly	Gln	Ala	Asp	Leu	Ala	Asp	Gly	991.4	991.3	8.00	3.44	11	>100
8	Gly	Gln	Leu	Ala	Leu	Ala	Asp	Gly	989.4	989.9	10.86	8.86	−1[e]	>200
9	Gly	Gln	Leu	Asp	Ala	Ala	Asp	Gly	991.4	991.9	7.33	3.44	7	>100
10	Gly	Gln	Leu	Asp	Leu	Ala	Ala	Gly	989.4	989.9	11.38	9.85	14	>100
11	Gly	Gln	Leu	Asp	Leu	Ala	Asp	Ala	1047.4	1047.5	11.65	10.12	15	>100
12	Gly	Glu	Leu	Asp	Leu	Ala	Asp	Gly	1034.4	1034.4	11.44	10.14	−2[e]	>200
13	Gly	Lys	Leu	Asp	Leu	Ala	Asp	Gly	1033.4	1033.6	10.13	7.78	−2[e]	>200
14	Gly	Asn	Leu	Asp	Leu	Ala	Asp	Gly	1019.4	1019.8	10.55	8.34	42	>100
15	Gly	Gln	Cha	Asp	Leu	Ala	Asp	Gly	1073.4	1073.4	13.40	14.44	−22	>100
16	Gly	Gln	Leu	Asp	Cha	Ala	Asp	Gly	1073.4	1073.4	13.61	14.68	10	>100
17	Gly	Gln	Leu	Asp	Leu	Gly	Asp	Gly	1019.4	1019.4	10.32	8.31	1[e]	>200
18	Gly	Gln	Leu	Asp	Leu	Ala	Asn	Gly	1032.4	1032.8	10.93	7.72	64	52

[a] Theoretical molecular mass (M + H^+, Da) except for **3** and **4**. [b] Observed molecular mass (M + H^+, Da) except for **3** and **4**. [c] (M − H^+, Da). [d] Retention time (see Experimental Section). [e] Synthetic peptides were assayed at 100 μM except for **8**, **12**, **13**, and **17** (at 200 μM).

At these positions, Leu would be suitable for the interaction with AP-1. Substitution of Ala7 with Gly (peptide **17**) resulted in a complete loss of inhibitory activity. The methyl side chain of Ala might participate in the interaction with AP-1, or the replacement with Gly might change the active conformation of the peptide to an inactive form.

Asp8 was substituted with Asn (peptide **18**), resulting in a moderate loss of inhibitory activity (6.5-fold). At this position, the charge–charge interaction with AP-1 would be more favorable. Of the peptides tested in this study, peptide **2** emerged as that with the most potent inhibitory activity against the binding of AP-1 to DNA.

Three-Dimensional Pharmacophore Modeling. To obtain 3D structural information for the active conformation of peptide **2**, we carried out a MD simulation of the bZIP–peptide **2** complex with explicit water molecules and NMR measurements of peptide **2** in water. The MD simulation was run for 400 ps until the system was equilibrated. Six snapshots, extracted at 10 ps intervals from the last 50 ps MD simulation, were similar to one another in terms of RMS deviation for all backbone N, C_α, C, and O atoms (mean ± SD = 1.85 ± 0.48 Å). Peptide **2** was stable during the last 50 ps of the MD simulation, and the average RMS deviations between each of the six snapshots for all backbone atoms and all heavy atoms were 0.65 ± 0.17 and 0.89 ± 0.13 Å, respectively.

The binding model of peptide **2** at 400 ps is presented in Figure 3. The leucine zipper region retained approximately 70% of the α-helical conformation at the carboxyl terminal, whereas the basic regions underwent a partial change to a random coil conformation, in particular for the c-Jun domain. This is similar to information obtained by CD and NMR about the solution structure of the AP-1 or GCN4 bZIP domains in the absence of DNA.[8,9] We speculate that the binding mode of peptide **2** with the bZIP domains is different from that of its binding to DNA.

The sequence-specific NMR assignment of peptide **2** was achieved according to the standard method established by Wüthrich.[37] Identification of amino acid spin systems was based on DQF-COSY[38] and TOCSY[39]

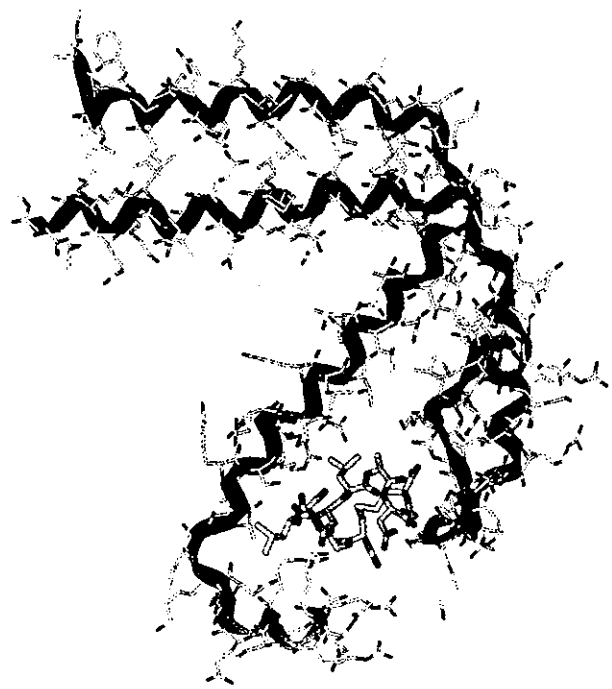

Figure 3. Binding model of peptide **2** (yellow) resulting from MD simulation at 400 ps. Ribbon representation of the bZIP domains (c-Fos, cyan; c-Jun, magenta).

spectra and complemented with the results of NOESY[40] experiments. Starting with the unique residue Ala7, which could be easily identified on the basis of its spin type, sequential connectivities were carried out by the analysis of the $C_\alpha H_{(i)}$–$NH_{(i+1)}$ ($d_{\alpha N}$) and $NH_{(i)}$–$NH_{(i+1)}$ nuclear Overhauser effects (NOEs). Figure 4 shows the C_αH–NH fingerprint region of the NOESY spectrum containing sequential $d_{\alpha N}$ connectivities. The proton chemical shifts of peptide **2** are summarized in Table 2.

For solution structure determination of peptide **2**, 12 intraresidual, 37 sequential, 19 medium range ($|i - j| < 5$, where i and j are residue numbers), and three long range ($|i - j| \geq 5$) NOEs were detected and converted to the distance constraints. On the basis of the ^3J(H-C_α-C_β-H) coupling constants and the intensities of

Table 2. ^{1}H Chemical Shifts[a] (ppm) for Peptide **2** at 5 °C and pH 4.65

residue	NH	H_α	H_β	others
CH_3[b]		2.02		
Cys1	8.62	4.64	3.00 (β2), 3.19 (β3)	
Gly2	8.89	3.95		
Gln3	8.37	4.26	1.98 (β2), 2.11 (β3)	C_γ 2.33; C_ϵ 6.92, 7.66
Leu4	8.33	4.28	1.57, 1.70	C_γ 1.57; C_δ 0.82, 0.88
Asp5	8.14	4.54	2.68, 2.84	
Leu6	8.17	4.29	1.58, 1.65	C_γ 1.57; C_δ 0.82, 0.88
Ala7	8.28	4.23	1.38	
Asp8	8.21	4.58	2.69 (β3), 2.77 (β2)	
Gly9	8.34	3.87, 4.02		
Cys10	8.25	4.60	3.00 (β2), 3.21 (β3)	
NH_2[b]	7.27, 7.77			

[a] Chemical shifts are relative to the water resonance located at 4.95 ppm. [b] Peptide **2** has an acetylated N terminus and an amidated C terminus.

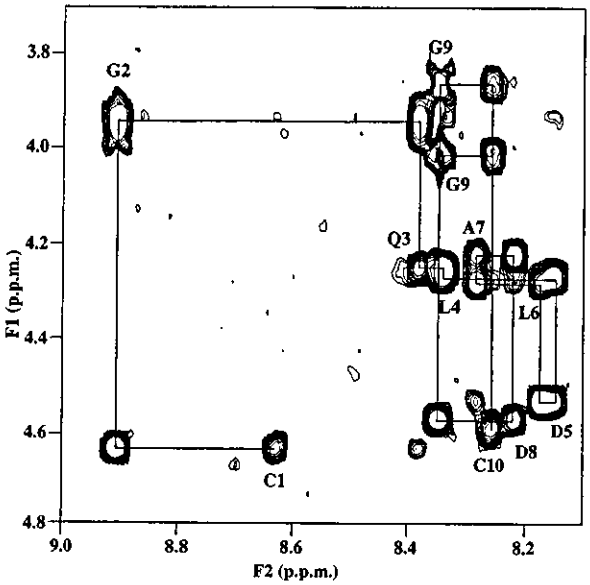

Figure 4. Sequential NOE connectivities for residues 1−10 of peptide **2** in the NOESY spectrum observed with a mixing time of 500 ms at 5 °C. Intraresidue NH-C_αH cross-peaks are labeled with the residue number by standard single-letter amino acid abbreviations.

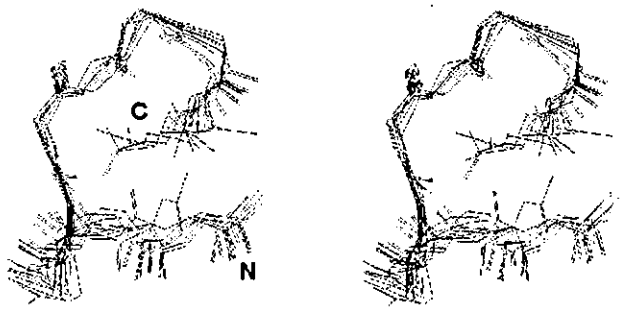

Figure 5. Stereoview of the superimposition of the 11 converged structures of the major cluster of peptide **2**. These are the results of the best fit of all backbone N, C_α, C, and O atoms.

intraresidual NOEs, we established the stereospecific assignments of the prochiral β-methylene protons and the range of the χ_1 side chain dihedral angles for Cys1, Gln3, Asp8, and Cys10. A total of 75 NMR constraints, which consisted of 71 distance constraints and four dihedral angle constraints, were used for the following simulated annealing calculations.

A set of 200 individual structures was calculated on the basis of the NMR experimental constraints. These

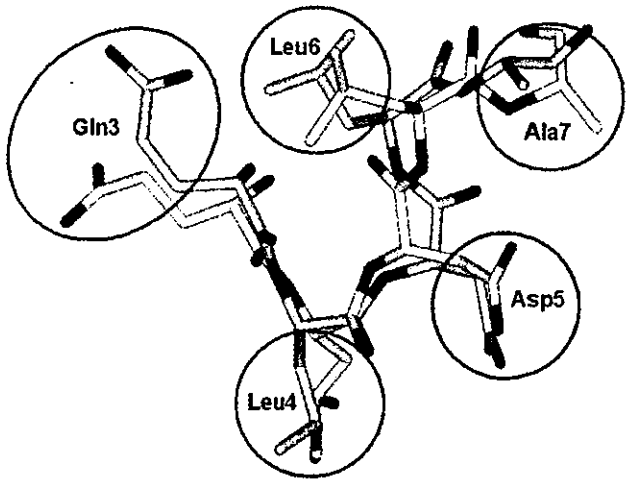

Figure 6. Superimposition of Gln3-Leu4-Asp5-Leu6-Ala7 of peptide **2** of the lowest energy conformer obtained by NMR (white) and MD simulation-derived structure at 400 ps (yellow). These are the results of the best fit of the backbone atoms. Three-dimensional pharmacophore model of AP-1 binding compounds: green, hydrophobic groups; blue, hydrogen donor or acceptor group; and red, acidic group.

calculations provided 17 structures that had no distance violations >0.2 Å and no dihedral angle violations >5°. The resulting conformations were grouped into three clusters according to the pairwise RMS deviations between 17 individual structures. Figure 5 shows a stereoview of the best-fit superimposition of the backbone atoms for the 11 individual converged structures of the major cluster. The average pairwise RMS deviation between the 11 structures was 1.18 ± 0.54 Å for all backbone atoms.

Here, we hypothesized that the rigid part of the cyclic peptide solution structure might be conserved in the biologically active conformation. Superimposition studies showed that the MD simulation-derived structures of peptide **2** in the complex were similar to the major cluster of the NMR-determined solution structures of peptide **2** in the backbones of the sequence Gln3-Leu4-Asp5-Leu6-Ala7 (1.45 ± 0.10 Å). Among these residues, the side chains of Glu3, Leu4, Asp5, and Leu6 have been shown by the alanine scan experiment to be important for inhibitory activity, as described above. Although it is unknown whether Ala7 is involved in the hydrophobic interaction with AP-1, we assumed that it contributes to the observed inhibitory activity.

From these results, we built a 3D pharmacophore model of AP-1 binding compounds, based on the chemi-

cal and structural features of the amino acid side chains of residues 3–7 in peptide **2** (Figure 6). The pharmacophore consists of three hydrophobic groups, one hydrogen bond acceptor or donor, and one acidic group. This 3D model will be useful in the process of molecular design and the search of 3D databases to identify the chemical structures of potential novel AP-1 inhibitors.

Conclusions

In the absence of precise 3D structural information about AP-1, a combination of the available experimental data and molecular modeling methods—such as docking and MD simulations—was used to design novel inhibitors of AP-1. The computer-aided molecular design strategies used in the present study produced novel cyclic decapeptides that exhibited AP-1 inhibitory activity. Such peptides will prove useful as intermediates in the search for nonpeptide and small molecule inhibitors.

This study proposes a 3D pharmacophore model of AP-1 binding compounds. We aim to use our model to discover small molecule inhibitors of AP-1 based on de novo design or 3D database searches. Although this model relies on many hypotheses and remains speculative, the current successful development of nonpeptide inhibitors lends credibility to the 3D pharmacophore model of AP-1 binding compounds.

Experimental Section

Abbreviations. Abbreviations of common amino acids and representations of peptides are in accordance with the recommendations of the IUPAC-IUB Joint Commission on Biochemical Nomenclature.[41] Additional abbreviations are used as follows: DMF, *N*,*N*-dimethylformamide; DMSO, dimethyl sulfoxide; Fmoc, 9-fluorenylmethoxycarbonyl; HPLC, high-performance liquid chromatography; mequiv, milliequivalent; *t*Bu, *tert*-butyl; TFA, trifluoroacetic acid; Trt, triphenylmethyl.

Materials and Methods. Rink Amide MBHA resin (0.55 mequiv/g) was obtained from NovaBiochem (Läufelfingen, Switzerland). All of the protected amino acids (Fmoc and Fmoc plus Trt or *t*Bu) and the coupling reagents were purchased from NovaBiochem. All purchased amino acids were of the L-configuration. All reagents and solvents were reagent grade or better and were used without further purification.

HPLC was performed with a Hitachi L-7100 apparatus equipped with an L-7400 UV detector (peak detection at 230 nm) using an ODS-AP column (YMC-Pack, YMC Co., Kyoto, Japan) of 250 mm × 20 mm for preparative or 150 mm × 4.6 mm for analytical HPLC, respectively. Liquid chromatography–electrospray ionization mass spectrometry was performed with a Finnigan 700 triple-sector quadrupole mass spectrometer equipped with a Waters 626 LC system and a Finnigan MAT electrospray ionization system (4.5 kV).

Peptide Synthesis. All peptides were synthesized manually using standard solid phase peptide chemistry[42] with Fmoc-protected amino acids[43] on Rink Amide MBHA resin[44] at a 0.2 mmol scale. Couplings with Fmoc amino acids (3 equiv) were performed in the presence of 1-hydroxybenzotriazole and 1,3-diisopropylcarbodiimide (each 3 equiv) in DMF (5 mL) at room temperature for 2 h, and then, the Fmoc protecting group was removed by treatment with 20% piperidine in DMF (5 mL) at room temperature for 20 min. After deprotection of the last Fmoc group on Cys(Trt), the peptide resin was treated with acetic anhydride and *N*,*N*-diisopropylethylamine (each 10 equiv) in a 1:1 mixture of DMF and CH_2Cl_2 (5 mL) at room temperature for 30 min before filtration and washing with DMF (×4) and CH_2Cl_2 (×3) followed by drying in vacuo. The terminal-N-acetyl product was treated with a mixture of TFA–thioanisole–water (92.5:5.0:2.5) (20 mL) at room temperature for 4 h to induce cleavage of the peptide from the resin and removal of the remaining O- and S-protecting groups. The exhausted resin was filtered, the filtrate was mixed with ether (50 mL), and the precipitate was isolated by centrifugation.

A solution of the dithiol product in 10% DMSO in TFA (10 mL) was stirred at room temperature for 20 h before concentration to approximately 2 mL and the addition of ether (50 mL).[45] The precipitate was collected by centrifugation and purified by preparative reverse phase HPLC eluted with a linear gradient of acetonitrile in water containing 0.1% TFA at a flow rate of 8.0 mL/min before lyophilization. The homogeneity of the resulting peptides was tested by analytical HPLC using two solvent systems: method 1, 30 min gradient of 10–70% acetonitrile in 0.1% aqueous TFA; method 2, 30 min gradient of 35–95% methanol in 0.1% aqueous TFA. The purity of the peptides was determined by HPLC to be >95%. A summary of the analytical results for each peptide described in this paper is provided in Table 1.

Enzyme-Linked DNA–Protein Interaction Assay. The inhibition constants of the synthetic peptides for DNA binding activity of AP-1 were determined by an enzyme-linked DNA–protein interaction assay using synthetic double-stranded oligonucleotides, which contain the AP-1 binding site (shown in bold) and nuclear protein. The synthetic oligonucleotides 5′-CTAGTGA**TGAGTCA**GCCGGATC-3′ and 5′-GATCCGGC-**TGACTCA**TCACTAG-3′ (Bio-Synthesis, Lewisville, TX) were labeled with DIG-ddUTP as described in the DIG oligonucleotide 3′-end-labeling kit (Boehringer Mannheim, Mannheim, Germany). After they were annealed, they were used as DIG-labeled double-stranded oligonucleotides. Nuclear extract proteins were prepared from phorbol myristate acetate-stimulated HeLa cells according to the protocol described by Dignam et al.[46] and were used after dialysis against reaction buffer [20 mM *N*-(2-hydroxyethyl)piperazine-*N*′-2-ethanesulfonic acid-KOH (pH 7.9) containing 0.5 mM ethylenediaminetetraacetic acid, 50 mM KCl, 0.5 mM dithiothreitol, 0.5 mM phenylmethylsulfonyl fluoride, and 10% (v/v) glycerol].

Ninety-six well microplates (Corning Inc., Corning, NY) were coated with nuclear extract (1 μg/mL; 100 μL/well) at 4 °C overnight. After they were washed with phosphate-buffered saline containing 0.05% Tween-20, DIG-labeled double-stranded oligonucleotides (10 pM) in reaction buffer were mixed with each sample dissolved in DMSO (99:1–98:2), and 100 μL of each mixture was added to the wells. After they were incubated for 1 h at room temperature, the wells were washed with reaction buffer containing 0.05% Tween-20. Horseradish peroxidase-conjugated goat anti-DIG antibody (0.04 units/mL, Boehringer Mannheim) in binding buffer containing 0.1% bovine serum albumin was added (100 μL/well) and incubated for 1 h at room temperature. *o*-Phenylenediamine (1 mg/mL) in 100 mM Na_2HPO_4/200 mM citric acid buffer (pH 5.0) containing 0.1% H_2O_2 was added (100 μL/well), and the color reaction was allowed to develop for 20 min at room temperature. After 50 μL of 1 M H_2SO_4 was added to each well to stop the reaction, the optical density was measured with a microplate reader (Bio-Rad model 450, Bio-Rad Laboratories, Hercules, CA) at a wavelength of 492 nm. The IC_{50} values were calculated by a logistic concentration–response curve using the SAS System version 8.2 (SAS Institute Inc., Cary, NA).

NMR Measurements and Simulated Annealing Calculations. Peptide **2** (4 mg) was dissolved in 0.5 mL of either 90% H_2O/10% D_2O or D_2O containing 50 mM CD_3COONa. The sample solution was adjusted to pH 4.65. All NMR spectra were recorded on a Varian INOVA600 spectrometer operating at 600 MHz for a proton frequency at two temperatures: 5 and 25 °C. For spectral assignment and extraction of structural information, DQF-COSY,[38] TOCSY,[39] NOESY,[40] ROESY,[47] and E.COSY[48] experiments were performed in the phase sensitive mode.[49] The DQF-COSY and E.COSY spectra were recorded with 512 increments of 8K data points and 32 transients. The TOCSY spectra were recorded with mixing times of 20 and 50 ms. The NOESY spectra were obtained with mixing times of 100, 200, 300, and 500 ms at 5 °C. The ROESY spectrum was obtained with a mixing time of 500 ms at 5 and 25 °C. Five

hundred twelve increments of 2K data points were recorded with 32−96 transients for the TOCSY, NOESY, and ROESY experiments. The solvent resonance was suppressed by selective irradiation during a relaxation delay of 2.0 s. The ^3J(H-C_α-C_β-H) measurement was carried out on an E.COSY spectrum recorded in D_2O. The chemical shifts were referenced with respect to H_2O, which in turn was calibrated using an internal standard, 2,2-dimethyl-2-silapentane-5-sulfonate, in a different sample. The chemical shift values of 4.95 and 4.75 ppm for the water signal were used at temperatures of 5 and 25 °C, respectively.

Interproton distance constraints were obtained from the NOESY spectra. Spin-diffusion effects were inspected by following the buildup of NOESY cross-peaks when mixing times were increased from 100 to 500 ms. The distance constraints were classified into four categories corresponding to 1.8−2.7, 1.8−3.5, 1.8−5.0, and 1.8−6.0 Å. Pseudoatoms were used for the prochiral methylene protons that had not been assigned in a stereospecific way, the methyl groups of the Ala and Leu residues and the C_α proton of the Gly residues.[50] Correction factors for the use of pseudoatoms were added to the distance constraints. In addition, 0.5 Å was added to the distance constraints involving methyl protons. All calculations were performed on a Silicon Graphics Octane workstation with the X-PLOR program.[51] The dynamical simulated annealing protocols were used to calculate the 3D structures.

Acknowledgment. This study was partially supported by the Japan Science and Technology Agency.

References

(1) Angel, P.; Karin, M. The Role of Jun, Fos and the AP-1 Complex in Cell-Proliferation and Transformation. *Biochim. Biophys. Acta* **1991**, *1072*, 129−157.
(2) Foletta, V. C.; Segal, D. H.; Cohen, D. R. Transcriptional Regulation in the Immune System: All Roads Lead to AP-1. *J. Leukocyte Biol.* **1998**, *63*, 139−152.
(3) Angel, P.; Baumann, I.; Stein, B.; Delius, H.; Rahmsdorf, H. J.; Herrlich, P. 12-*O*-Tetradecanoyl-Phorbol-13-Acetate Induction of the Human Collagenase Gene Is Mediated by an Inducible Enhancer Element Located in the 5′-Flanking Region. *Mol. Cell. Biol.* **1987**, *7*, 2256−2266.
(4) Suto, M. J.; Ransone, L. J. Novel Approaches for the Treatment of Inflammatory Diseases: Inhibitors of NF-κB and AP-1. *Curr. Pharm. Des.* **1997**, *3*, 515−528.
(5) Shiozawa, S.; Shimizu, K.; Tanaka, K.; Hino, K. Studies on the Contribution of c-fos/AP-1 to Arthritic Joint Destruction. *J. Clin. Invest.* **1997**, *99*, 1210−1216.
(6) Kouzarides, T.; Ziff, E. The Role of the Leucine Zipper in the Fos-Jun Interaction. *Nature* **1988**, *336*, 646−651.
(7) Glover, J. N. M.; Harrison, S. C. Crystal Structure of the Heterodimeric bZIP Transcription Factor c-Fos-c-Jun Bound to DNA. *Nature* **1995**, *373*, 257−261.
(8) Patel, L.; Abate, C.; Curran, T. Altered Protein Conformation on DNA Binding by Fos and Jun. *Nature* **1990**, *347*, 572−575.
(9) Saudek, V.; Pastore, A.; Morelli, M. A. C.; Frank, R.; Gausepohl, H.; Gibson, T.; Weih, F.; Roesch, P. Solution Structure of the DNA-Binding Domain of the Yeast Transcriptional Activator Protein GCN4. *Protein Eng.* **1990**, *4*, 3−10.
(10) Gohlke, H.; Klebe, G. Approaches to the Description and Prediction of the Binding Affinity of Small-Molecule Ligands to Macromolecular Receptors. *Angew. Chem., Int. Ed.* **2002**, *41*, 2644−2676.
(11) Davis, A. M.; Teague, S. J.; Kleywegt, G. J. Application and Limitations of X-ray Crystallographic Data in Structure-Based Ligand and Drug Design. *Angew. Chem., Int. Ed.* **2003**, *42*, 2718−2736.
(12) Lee, S.; Park, S.; Jun, G.; Hahm, E.-R.; Lee, D.-K.; Yang, C.-H. Quantitative Assay for the Binding of Jun-Fos Dimer and Activator Protein-1 Site. *J. Biochem. Mol. Biol.* **1999**, *32*, 594−598.
(13) Hahm, E.-R.; Cheon, G.; Lee, J.; Kim, B.; Park, C.; Yang, C.-H. New and Known Symmetrical Curcumin Derivatives Inhibit the Formation of Fos-Jun-DNA Complex. *Cancer Lett.* **2002**, *184*, 89−96.
(14) Park, S.; Lee, D.-K.; Yang, C.-H. Inhibition of Fos-Jun-DNA Complex Formation by Dihydroguaiaretic Acid and in Vitro Cytotoxic Effects on Cancer Cells. *Cancer Lett.* **1998**, *127*, 23−28.
(15) Park, S.; Lee, D. K.; Whang, Y. H.; Yang, C. H. Momordin I, a Compound of Ampelopsis Radix, Inhibits AP-1 Activation Induced by Phorbol Ester. *Cancer Lett.* **2000**, *152*, 1−8.
(16) Goto, M.; Masegi, M.; Yamauchi, T.; Chiba, K.; Kuboi, Y.; Harada, K.; Naruse, N. K1115 A, a New Anthraquinone Derivative that Inhibits the Binding of Activator Protein-1 (AP-1) to its Recognition Sites. *J. Antibiot.* **1998**, *51*, 539−544.
(17) Ghose, A. K.; Wendoloski, J. J. Pharmacophore Modelling: Methods, Experimental Verification and Applications. *Perspect. Drug Discovery Des.* **1998**, 253−271.
(18) Hruby, V. J. Conformational and Topographical Considerations in the Design of Biologically Active Peptides. *Biopolymers* **1993**, *33*, 1073−1082.
(19) Li, P.; Roller, P. P. Cyclization Strategies in Peptide Derived Drug Design. *Curr. Top. Med. Chem.* **2002**, *2*, 325−341.
(20) *SYBYL 6.4*; Tripos, Inc.: St. Louis, MO, 1997.
(21) Nakabeppu, Y.; Nathans, D. The Basic Region of Fos Mediates Specific DNA Binding. *EMBO J.* **1989**, *8*, 3833−3841.
(22) Turner, R.; Tjian, R. Leucine Repeats and an Adjacent DNA Binding Domain Mediate the Formation of Functional cFos-cJun Heterodimers. *Science* **1989**, *243*, 1689−1694.
(23) Gentz, R.; Rauscher, F. J., III; Abate, C.; Curran, T. Parallel Association of Fos and Jun Leucine Zippers Juxtaposes DNA Binding Domains. *Science* **1989**, *243*, 1695−1699.
(24) Neuberg, M.; Schuermann, M.; Hunter, J. B.; Müller, R. Two Functionally Different Regions in Fos are Required for the Sequence-Specific DNA Interaction of the Fos/Jun Protein Complex. *Nature* **1989**, *338*, 589−590.
(25) Risse, G.; Jooss, K.; Neuberg, M.; Brüller, H.-J.; Müller, R. Asymmetrical Recognition of the Palindromic AP1 Binding Site (TRE) by Fos Protein Complexes. *EMBO J.* **1989**, *8*, 3825−3832.
(26) Ransone, L. J.; Visvader, J.; Wamsley, P.; Verma, I. M. Trans-Dominant Negative Mutants of Fos and Jun. *Proc. Natl. Acad. Sci. U.S.A.* **1990**, *87*, 3806−3810.
(27) Clark, M.; Cramer, R. D, III; Van Opdenbosch, N. Validation of the General Purpose Tripos 5.2 Force Field. *J. Comput. Chem.* **1989**, *10*, 982−1012.
(28) Gasteiger, J.; Marsili, M. Iterative Partial Equalization of Orbital Electronegativity—A Rapid Access to Atomic Charges. *Tetrahedron* **1980**, *36*, 3219−3228.
(29) Purcell, W. P.; Singer, J. A. A Brief Review and Table of Semiempirical Parameters Used in the Hückel Molecular Orbital Method. *J. Chem. Eng. Data* **1967**, *12*, 235−246.
(30) Pearlman, D. A.; Case, D. A.; Caldwell, J. W.; Ross, W. S.; Cheatham, T. E., III; Ferguson, D. M.; Seibel, G. L.; Singh, U. C.; Weiner, P.; Kollman, P. A. *AMBER 4.1*; University of California: San Francisco, CA, 1995.
(31) Jorgensen, W. L.; Chandrasekhar, J.; Madura, J. D.; Impey, R. W.; Klein, M. L. Comparison of Simple Potential Functions for Simulating Liquid Water. *J. Chem. Phys.* **1983**, *79*, 926−935.
(32) Ryckaert, J.-P.; Ciccotti, G.; Berendsen, H. J. C. Numerical Integration of the Cartesian Equations of Motion of a System with Constraints: Molecular Dynamics of *n*-Alkanes. *J. Comput. Phys.* **1977**, *23*, 327−341.
(33) Peeters, T. L.; Macielag, M. J.; Depoortere, I.; Konteatis, Z. D.; Florance, J. R.; Lessor, R. A.; Galdes, A. D-Amino Acid and Alanine Scans of the Bioactive Portion of Porcine Motilin. *Peptides* **1992**, *13*, 1103−1107.
(34) Tam, J. P.; Liu, W.; Zhang, J.-W.; Galantino, M.; Bertolero, F.; Cristiani, C.; Vaghi, F.; De Castiglione, R. Alanine Scan of Endothelin: Importance of Aromatic Residues. *Peptides* **1994**, *15*, 703−708.
(35) Sahm, U. G.; Olivier, G. W. J.; Branch, S. K.; Moss, S. H.; Pouton, C. W. Synthesis and Biological Evaluation of α-MSH Analogues Substituted with Alanine. *Peptides* **1994**, *15*, 1297−1302.
(36) Leprince, J.; Gandolfo, P.; Thoumas, J.-L.; Patte, C.; Fauchère, J.-L.; Vaudry, H.; Tonon, M.-C. Structure−Activity Relationships of a Series of Analogues of the Octadecaneuropeptide ODN on Calcium Mobilization in Rat Astrocytes. *J. Med. Chem.* **1998**, *41*, 4433−4438.
(37) Wüthrich, K. *NMR of Proteins and Nucleic Acids*; John Wiley & Sons: New York, 1986.
(38) Rance, M.; Sørensen, O. W.; Bodenhausen, G.; Wagner, G.; Ernst, R. R.; Wüthrich, K. Improved Spectral Resolution in COSY ^{1}H NMR Spectra of Proteins via Double Quantum Filtering. *Biochem. Biophys. Res. Commun.* **1983**, *117*, 479−485.
(39) Bax, A.; Davis, D. G. MLEV-17-Based Two-Dimensional Homonuclear Magnetization Transfer Spectroscopy. *J. Magn. Reson.* **1985**, *65*, 355−360.
(40) Macura, S.; Huang, Y.; Suter, D.; Ernst, R. R. Two-Dimensional Chemical Exchange and Cross-Relaxation Spectroscopy of Coupled Nuclear Spins. *J. Magn. Reson.* **1981**, *43*, 259−281.
(41) IUPAC-IUB Joint Commission on Biochemical Nomenclature (JCBN) Nomenclature and Symbolism for Amino Acids and Peptides. *J. Biol. Chem.* **1985**, *260*, 14−42.
(42) Merrifield, R. B. Solid Phase Peptide Synthesis. I. The Synthesis of a Tetrapeptide. *J. Am. Chem. Soc.* **1963**, *85*, 2149−2154.

(43) Carpino, L. A.; Han, G. Y. The 9-Fluorenylmethoxycarbonyl Amino-Protecting Group. *J. Org. Chem.* **1972**, *37*, 3404−3409.
(44) Rink, H. Solid-Phase Synthesis of Protected Peptide Fragments Using a Trialkoxy-Diphenyl-Methylester Resin. *Tetrahedron Lett.* **1987**, *28*, 3787−3790.
(45) Otaka, A.; Koide, T.; Shide, A.; Fujii, N. Application of Dimethylsulphoxide (DMSO)/Trifluoroacetic Acid (TFA) Oxidation to the Synthesis of Cystine-Containing Peptide. *Tetrahedron Lett.* **1991**, *32*, 1223−1226.
(46) Dignam, J. D.; Lebovitz, R. M.; Roeder, R. G. Accurate Transcription Initiation by RNA Polymerase II in a Soluble Extract from Isolated Mammalian Nuclei. *Nucleic Acids Res.* **1983**, *11*, 1475−1489.
(47) Bax, A.; Davis, D. G. Practical Aspects of Two-Dimensional Transverse NOE Spectroscopy. *J. Magn. Reson.* **1985**, *63*, 207−213.
(48) Griesinger, C.; Sørensen, O. W.; Ernst, R. R. Practical Aspects of the E.COSY Technique. Measurement of Scalar Spin−Spin Coupling Constants in Peptides. *J. Magn. Reson.* **1987**, *75*, 474−492.
(49) States, D. J.; Haberkorn, R. A.; Ruben, D. J. A Two-Dimensional Nuclear Overhauser Experiment with Pure Absorption Phase in Four Quadrants. *J. Magn. Reson.* **1982**, *48*, 286−292.
(50) Wüthrich, K.; Billeter, M.; Braun, W. Pseudo-Structures for the 20 Common Amino Acids for Use in Studies of Protein Conformations by Measurements of Intramolecular Proton−Proton Distance Constraints with Nuclear Magnetic Resonance. *J. Mol. Biol.* **1983**, *169*, 949−961.
(51) Brünger, A. T. *X-PLOR version 3.1*; Yale University: New Haven, CT, 1993.

JM049890+

Genes and Immunity (2004) 5, 439–443

www.nature.com/gene

FULL PAPER

Death receptor 3 (DR3) gene duplication in a chromosome region 1p36.3: gene duplication is more prevalent in rheumatoid arthritis

K Osawa[1,2], N Takami[1,2], K Shiozawa[3], A Hashiramoto[1,2,4] and S Shiozawa[1,2,4,5]
[1]*Department of Rheumatology, Kobe University FHS School of Medicine, Kobe, Japan;* [2]*Division of Bioregulation, Kobe University Graduate School of Medicine, Kobe, Japan;* [3]*Department of Rheumatology, Konan Kakogawa Hospital, Kakogawa, Japan;* [4]*Rheumatic Diseases Division, Kobe University Hospital, Kobe, Japan;* [5]*Investigator of the Center of Excellence (COE), Japan*

The death receptor 3 (DR3) gene is a member of the apoptosis-inducing Fas gene family. In the current study, fluorescence in situ hybridization (FISH) and Fiber-FISH revealed the existence of a second DR3 gene ~200 kb upstream of the original DR3 gene. The existence of the duplicated DR3 gene was confirmed by sequencing the corresponding human artificial chromosome clones as well as with quantitative PCR that measured the ratio of the DR3 gene mutation (Rm), intrinsic to rheumatoid arthritis (RA) patients, by simultaneous amplification of the normal and mutated DR3 sequences. The DR3 gene duplication measured by FISH was found to be more frequent in patients with RA as compared to healthy individuals. We therefore surmise that the human DR3 gene can be duplicated and that this gene duplication is more prevalent in patients with RA.
Genes and Immunity (2004) **5**, 439–443. doi:10.1038/sj.gene.6364097
Published online 8 July 2004

Keywords: *gene duplication; death receptor 3 (DR3); fluorescence in situ hybridization (FISH); rheumatoid arthritis (RA)*

Introduction

The death receptor 3 (DR3), also named Ws1, Apo3, TRAMP, LARD, TR3 or TNFRSF25, is a member of the tumor necrosis factor receptor (TNFR) superfamily which includes CD95/Fas, TNFR1, DR4, DR5 and DR6.[1,2] DR3 contains four characteristic cysteine-rich motifs as well as a death domain capable of inducing cellular apoptosis and proliferation.[3,4] We previously assigned three principal chromosome regions of linkage, D1S253/214, D8S556 and DXS1232, with maximum lod scores (MLSs) 3.77/6.13, 4.20/1.14 and 2.35/3.03, respectively, by single/multi-point analyses.[5] The death receptor 3 (*DR3*) gene was mapped in the vicinity of D1S214/253 by the GeneBridge 4.0 radiation hybrid panel. Based on the EBI/Sanger Institute ENSEMBL database, D1S214 and D1S253 reside at 6.7 and 6.0 Mb, respectively, and *DR3* at 6.2 Mb of chromosome 1p36. We subsequently identified a polymorphism in the *DR3* gene containing four single-nucleotide polymorphisms (SNPs) and one locus of a 14 nucleotide deletion within exon 5 and intron 5: g.1755A>G, g.2457_2470delT14, g.2531C>T, g.2678A>T and g.2826A>G (GenBank accession nos. AB051850 to *DR3* and AB051851 to mutant *DR3*). These polymorphisms were found to be genetically associated with rheumatoid arthritis (RA).[6]

Correspondence: Dr S Shiozawa, Department of Rheumatology, Kobe University FHS School of Medicine, 7-10-2 Tomogaoka, Sumaku, Kobe 654-0142, Japan. E-mail: shioz@kobe-u.ac.jp
Received 06 February 2004; revised 31 March 2004; accepted 31 March 2004; published online 8 July 2004

The current study examines the location of the *DR3* gene based on the previous findings of Grenet *et al*,[7] who showed that the *DR3* gene was duplicated and tandemly located in 1p36.2–1p36.3 in one male healthy donor. The authors suggested that duplicated genes are hemizygously deleted and/or possibly translocated to another chromosome as revealed in neuroblastoma cell lines. Using FISH, DNA sequencing and quantitative PCR, we demonstrate here that the human *DR3* gene can be duplicated and that the duplicated *DR3* gene is located ~200 kb upstream of the original *DR3* gene sequence. These findings are discussed in relation to the increased frequency of gene duplication found in patients with RA.

Results and discussion

Visual imaging

To locate the *DR3* gene using FISH, we used two probes, P1-derived artificial chromosome (PAC) clone 650H14 (GenBank accession no. AL158217) containing the *DR3* gene and control PAC 126A5 (GenBank accession no. AL031447), each spanning the region between D1S214 and D1S253 (Figure 1a). We found that the number of fluorescent signals derived from PAC 650H14 was between 2 and 4 (Figure 1b), whereas the number of signals from PAC 126A5 was exactly 2, suggesting the existence of gene duplication in the chromosome region containing the *DR3* gene.

We tried to confirm this by using the Fiber-FISH technique. The result showed that the PAC 650H14 (green) and PAC 126A5 (red) hybridization signals were located in tandem. Interestingly, one additional green

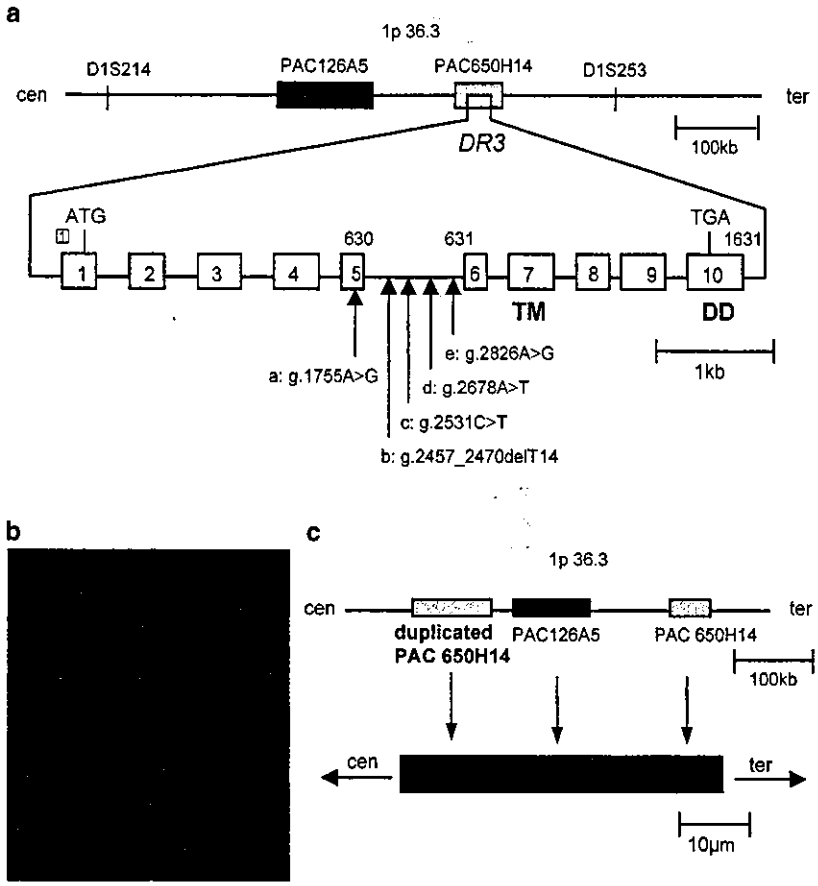

Figure 1 FISH and Fiber-FISH study. (a) Location of PAC 650H14 clone containing the *DR3* gene and control PAC 126A5 clone. We performed FISH using PAC clone 650H14 (54 kb) and PAC 126A5 (112 kb). According to the NCBI and EBI/Sanger Institute ENSEMBL databases, PAC 650H14 contains the *DR3* gene. Location of *DR3* mutation was depicted in relation to transmembrane (TM) and death domain (DD) portions. a: g.1755A>G, b: g.2457_2470delT14, c: g.2531C>T, d: g.2678A>T and e: g.2826A>G (GenBank accession no. AB051850) corresponded to a: g.3658A>G, b: g.4360_4373delT14, c: g.4434C>T, d: g.4581A>T and e: g.4729A>G according to GenBank accession no. AY254324. Numbered boxes represented exons. cDNA nucleotide and amino acid numbered according to Marsters *et al*.[4] (b) FISH imaging by using rhodamine-labeled PAC 650H14. Human peripheral blood mononuclear cells (PBMC), cultured with 10 μg/ml of phytohaemagglutinin (PHA) for 72 h, were treated with 40 ng/ml of colcemid for 15 min and a hypotonic 75 mM KCl solution at 37°C for 20 min, followed by fixation in methanol-acetate (3:1). A drop of fixed cell suspension was placed on a glass slide at 72°C and air-dried. DNA of PAC clones was labeled by nick translation with biotin-16-dUTP or digoxigenin-11-dUTP. The slides of metaphase chromosomes were denatured, dehydrated and air-dried. Denatured biotin- or digoxigenin-labeled DNA probes were then applied and hybridized signals were detected with avidin-FITC and biotinylated anti-avidin D for biotin-labeled probes or with Fab fragment of rhodamine-labeled anti-digoxigenin-fluorescein for digoxigenin-labeled probes. After counter-staining with 4′,6-diamidino-2-phenylindole dihydrochloride (DAPI), more than 20 metaphase chromosomes were analyzed for the hybridization signals for each sample under Laser Scan Microscope LSM510 (Carl Zeiss GmbH, Stuttgalt, Germany). Four red dots indicated duplicated *DR3* genes (arrows). (c) Fiber-FISH signal of PAC 126A5 (red) and PAC 650H14 (green) clones. For chromatin DNA fiber stream preparation (Fiber-FISH), glass slides containing a drop of fixed cell suspension were placed in phosphate-buffered saline, and a solution containing NaOH and ethanol was dragged over the cells using the short edge of a long coverslip. The slides were rinsed with methanol, air-dried and observed under LSM510.[16,17] The position of duplicated gene revealed in relation to original PAC 650H14 and PAC 126A5 clones in a short chromosome 1p36.3 region prepared from a representative patient with RA.

signal from PAC 650H14 was found in the upstream region of the DNA fiber towards the microsatellite marker D1S214 (Figure 1c). As all signal lengths were normalized according to the size of the probes (~0.01 μm/kb), the location of the duplicated region of PAC 650H14 was estimated to be ~200 kb upstream of the original PAC 650H14 towards the direction of the centromere. This type of gene duplication was not observed for PAC 126A5 or for the chromosomes containing only one *DR3* allele as revealed by FISH. The *DR3* gene duplication was not clearly assigned in the NCBI and the EBI/Sanger Institute ENSEMBL databases.

Gene duplication has been frequently reported in this area of 1p36. First, Grenet *et al*[7] registered a small region encompassing *DR3* as TNFRSF12L to the NCBI database without exactly locating its position. They simultaneously reported in a separate manuscript, however, that the *DR3* gene as well as a duplicate copy of the gene were both located at 1p36 and separated by several megabases. Second, Gururajan *et al*[8] reported that the human *Cdc2L1* and *Cdc2L2* genes, encoding almost identical protein kinases, were located at 1p36 in close proximity to *p73* and that the two genes were separated by only ~50 kb. Third, the two genes of the human Rhesus (RH) blood group locus, *RHD* and *RHCE*, also located in 1p36.1, are separated by less than 200 kb.[9] Therefore, we surmise that the 1p36.2 and 1p36.3 regions, which contain a number of other members of the apoptotic gene family, including

TNFRII,[10] CD30,[11] OX40[12] and 4-1BB[13], are subject to a similar phenomenon, and that gene duplication, if present, is not unique to the *DR3* gene.

Study of artificial clones

Query of the NCBI database revealed the existence of seven PAC and BAC clones of human chromosome 1 genomic contig that encompassed D1S214 and D1S253. We sequenced the DNA of PAC 650H14, PAC 126A5, PAC 202O8 (GenBank accession no. AL031848), bacterial artificial chromosome (BAC) clone 58A11 (GenBank accession no. AL591866), BAC 239P22 (GenBank accession no. AL159177), BAC 242F24 (GenBank accession no. AL591163) and BAC 312B8 (GenBank accession no. AL590128) located between D1S253 and D1S214 in chromosome 1p36.3 (Figure 2a). Sequencing showed that PAC 125A5, BAC 239P22, BAC 242F24 and BAC 312B8 are located in tandem, with a certain proportion of overlapping sequence among them (Figure 2a). The results showed that D1S214 was contained in the BAC 312B8 clone. We next sequenced all the seven artificial clones within the DR3 region and compared the results to the known *DR3* cDNA sequence.[3] We amplified seven genomic fragments A, B, C, D, E, F and G as shown in Figure 2b. In doing this, we found that, together, PAC 650H14 and BAC 58A11 contained the entire *DR3* gene sequence. While both of these clones have not been previously reported to contain the *DR3* gene, the NCBI database notes that the reported sequence did not include the entire insert sequences in the BAC 58A11 sequence. We may therefore assign the *DR3* gene to PAC 650H14.

We also found a portion of the BAC 239P22 sequence overlapped with PAC 126A5 (1–2000 bp). We determined through DNA sequencing that BAC 239P22 also contained the complete *DR3* gene sequence. It again appears that the previously reported sequence in the NCBI database did not represent the entire insert sequence in the BAC 239P22 sequence. In studying this clone, we identified two loci of four-nucleotide and eight-nucleotide deletions within exon 1, as well as two SNPs in exon 1 and intron 6 (Figure 2b). As was the case for the original *DR3* gene, we had difficulty in amplifying the 78 bp region containing poly T sequences within intron 5, possibly due to polymerase slippage. We found that BAC 239P22 did not overlap with BAC 58A11, because (1) PAC 126A5 did not overlap with BAC 58A11, and (2) another gene called *FLJ10737* existed in between the PAC

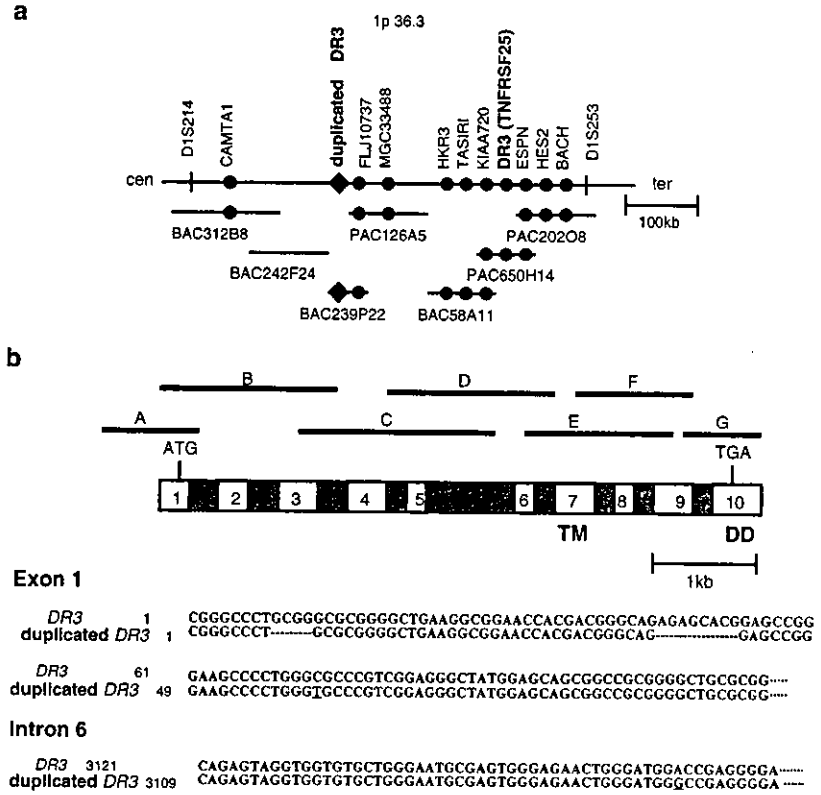

Figure 2 Study of artificial clones. (**a**) Location of original and duplicated *DR3* genes, three PAC clones (650H14, 126A5, 202O8) and four BAC clones (58A11, 239P22, 242F24, 312B8) in relation to D1S214 and D1S253. Black dots represented overlapped identical genes, and a rhombus represented a newly identified duplicated *DR3* gene. (**b**) Structure and sequence of original and duplicated *DR3* genes, as sequenced from human PAC and BAC clones by using probes A–G. The primers used for amplifying the *DR3* gene were: 5′-TTGAAGTGGTTCTCAGGGTT-3′ (forward) and 5′-CTCTTGGGACAGGGCTCAAAGCT-3′ (reverse) for region A; 5′-CTGAAGGCGGAACCACGA-3′ (forward) and 5′-AGGCGAAAGACAGACAGGTACAG-3′ (reverse) for region B; 5′-GCCTGGGAGAACCACCATAATTCTG-3′ (forward) and 5′-CCACAGACACTATTCACTGAGC-3′ (reverse) for region C; 5′-GCCAGGCTGGTTTGTGGA-3′ (forward) and 5′-TCCATCCCAGTTCTCCCAC-3′ (reverse) for region D; 5′-GCTGTCTGTGGCTGGAGGC-3′ (forward) and 5′-TCTCACTGCTGTCAGGAGGTGCT-3′ (reverse) for region E; 5′-GATTCGTACACAGGAGCTAACAGTTC-3′ (forward) and 5′-AGCTGTTACCCACCAACTGGAC-3′ (reverse) for region F; and 5′-GTCCAGTTGGTGGGTAACAGCTGGA-3′ (forward) and 5′-AGCGCTTGAGCATCTCGTACTGC-3′ (reverse) for region G. The PCR products were directly sequenced in an ABI 3700 sequencer (Applied Biosystems, Lincoln Centre Drive Foster City, CA, USA) using the BigDye Terminator Cycle Sequencing kit. Mutated nucleotides are underlined.

126A5 and BAC 239P22 clones. The reported DNA sequence of *FLJ10737* was found in tandem without interruption in the PAC 126A5 and BAC 239P22 clones in Homo sapiens chromosome 1 genomic contig (GenBank accession no. NT_028054). In addition, our DNA fiber stream preparation (Fiber-FISH) showed that the PAC 126A5 signal was located exactly upstream of the original PAC 650H14, in the direction of D1S214 and the centromere (Figure 1c). Together, we conclude from these findings that the *DR3* gene contained in the BAC 239P22 clone is a duplicate copy of the original *DR3* gene.

Study of the ratio of mutation

The ratio of mutation (Rm), intrinsic to the *DR3* gene in patients with RA,[6] was measured by simultaneously amplifying normal and mutated *DR3* DNA from RA patients whose genetic polymorphism was confirmed by sequencing. It can normally be expected that the Rm will be 0, 50 and 100% among individuals with the genotypes +/+, mt/+ and mt/mt, respectively; where mt represents the individuals with the haplotypes a: g.1755A>G, b: g.2457_2470delT14, c: g.2531C>T, d: g.2678A>T and e: g.2826A>G (Figure 1a). The result showed that, while the Rm of individuals with + / + ($n=30$) was exactly 0%, the Rm of those with mt/mt was 95.1% for SNPa and 84.2% for SNPd, respectively (Figure 3a). The Rm of those with mt/ + was 45.6±24.3% (13.5–82.2%) ($n=6$) for the SNPa locus and 40.6±16.2% (24.7–66.6%) ($n=6$) for the SNPd locus. If the gene was in single copy, the Rm of those with mt/ + should be exactly 50% (Figure 3b). However, as shown in Figure 3a, the Rm of those with mt/ + was evenly distributed at 25, 50 and 75% with a focus on 50%. The results therefore support a gene duplication model.

Frequency of gene duplication

Further, more than 20 metaphase chromosomes per person were scored using FISH and the mean allele number observed for each individual was plotted. A

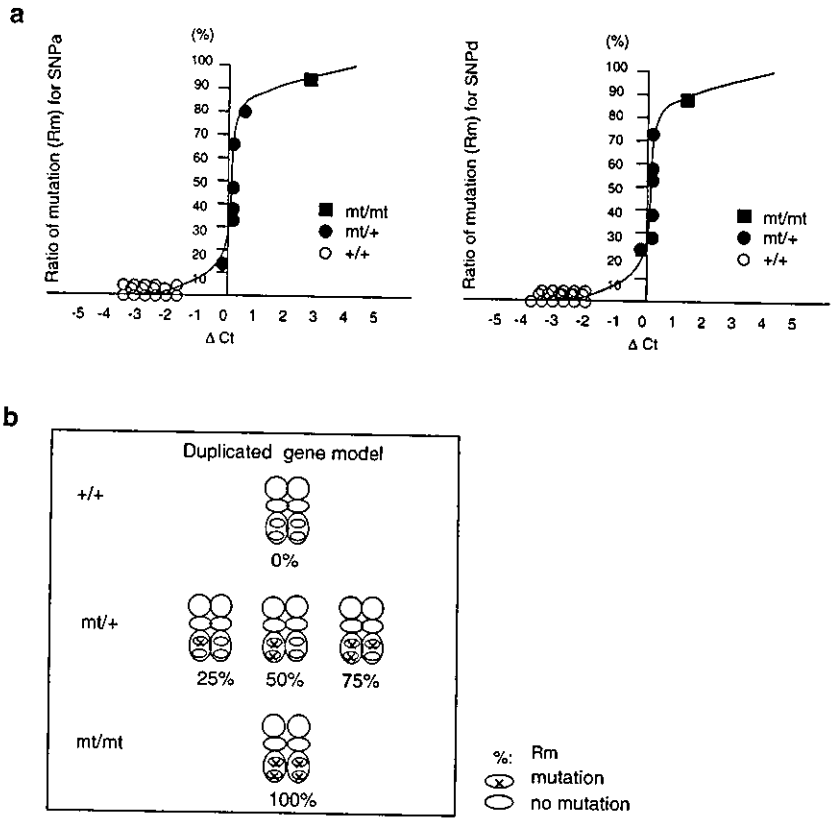

Figure 3 Quantitative PCR study of the ratio of mutation (Rm). (**a**) The Rm for SNPa (left) and SNPd (right) locus of *DR3* gene[6] in the individuals with genotypes + / + (open circle) ($n=30$), mt/ + (closed circle) ($n=6$) and mt/mt closed (square). To determine the ratio of mutation (Rm) for the *DR3* gene, we measured the allele frequencies for each of the target genes using the methods as described by Germer *et al*.[18] The Rm was calculated by using ΔCt of quantitative PCR. The quantitative PCR reactions used either a normal (Reaction I) or a mutated forward primer (Reaction II, 3′-portion of sense primer specific for disease-associated SNP) in conjunction with a common reverse primer and SYBR Green PCR Master Mix reagent containing uracil-N-glycosylase (UNG). A standard curve was constructed by amplifying in an ABI PRISM 7700 (Applied Biosystems) 0:100, 20:80, 25:75, 33:66, 50:50, 66:33, 75:25, 80:20 and 100:0 mixtures of normal *vs* mutated *DR3* exons 4–7 that had been subcloned into the pT7Blue vector (Novagen). The PCR thermal cycling conditions were as follows: a pre-run of 50°C for 2 min and 95°C for 12 min, followed by 45 cycles at 95°C for 20 s and 58°C for 20 s, and a final incubation at 72°C for 20 min. When the ratio of mixed plasmids (simulating a range of Rm) was plotted on the *y*-axis and ΔCt was plotted on the *x*-axis, a standard S-shaped curve was obtained. The ratio of mutation (Rm) was expressed as $Rm = \exp(\Delta Ct)/(1+\exp(\Delta Ct))$, where ΔCt = (Ct of Reaction I)−(Ct of Reaction II). Genomic DNA was then quantified accordingly. The primers were: 5′-CAGGTTCCCGCAGAGA-3′ (forward; normal) or 5′-CAGGTTCCCGCAGAGG-3′ (forward; mutated), and 5′-CCACGACAGCTAGGAATTACGT-3′ (reverse) for SNPa; 5′-GCCAAGATGGTCTTGATCA-3′ (forward; normal) or 5′-TAGCCAAGATGGTCTTGATCT-3′ (forward; mutated), and 5′-GCACCTAGAACAGTGTGTAGAACATAGCA-3′ (reverse) for SNPd (Figure 1a). (**b**) Distribution of Rm among individuals fitted a duplicated gene model.

Table 1 Frequency of *DR3* gene duplication

	N	*With gene duplication*	*Without gene duplication*	χ^2	*OR (95% CI)*
Healthy individuals	28	11 (0.39)	17 (0.61)	$P=0.01$	5.56 (1.60–19.4)
Rheumatoid patients	23	18 (0.78)	5 (0.22)		

N, number of individuals studied. Parenthesis, proportion. OR, odds ratio. Metaphase chromosome spreads were prepared and processed for FISH. The patients with RA fulfilling the diagnostic criteria of the American College of Rheumatology and their pedigrees[19] or geographically and ethnically similar healthy individuals living in the same distinct, Hyogo prefecture, Japan, were compared, under the written consent based on certification of the ethical board of Kobe University Graduate School of Medicine. Healthy individuals, $n=28$ (14 males; 14 females), and rheumatoid patients, $n=23$ (four males; 19 females).

result was obtained if >60% of the score value fell into either the duplicated or no duplicated category. The frequency of *DR3* gene duplication using this method was 78% (18/23) in patients with RA and 39% (11/28) in healthy individuals ($P=0.01$, odds ratio 5.56) (Table 1). The finding may be in line with Ohno's proposal that gene duplication can be a prerequisite for evolution.[14] We found that disease-associated *DR3* haplotype containing four SNPs and one 14 nucleotide deletion within exon 5 and intron 5 was significantly concentrated in a population of Japanese familial patients with RA as compared with healthy control ($P<0.0006$),[6] which may imply that, while the vast majority of gene duplicates are silenced within a few million years of evolution, gene duplication also has the potential to generate substantial molecular substrate for the origin of evolutional novelties.[15]

Acknowledgements

We thank Professor J Inazawa and Dr F Saito-Ohara at the Tokyo medical and dental University for their technical advise on FISH and Fiber-FISH, and Drs Y Konishi, H Kawasaki, Y Miura, K Komai and K Murayama at Kobe University for useful advice. We also thank Dr M Lamphier for critical reading of the manuscript. This study is expected to be a doctoral thesis of KO. This investigation was supported in part by a Grand-in-Aid for Scientific Research of the Ministry of Education, Culture, Sports, Science and Technology of Japan, Nos. 14657117 to KO and 13204059 to SS. This research was also supported by a grant for 21st Century COE Program, 'Center of Excellence for Signal Transduction disease: Diabetes Mellitus as Model' from the Ministry of Education, Culture, Sports, Science and Technology of Japan to SS.

References

1 Locksley RM, Killeen N, Lenardo MJ. The TNF and TNF receptor superfamilies: integrating mammalian biology. *Cell* 2001; **104**: 487–501.
2 Kitson J, Raven T, Jiang YP *et al*. A death-domain-containing receptor that mediates apoptosis. *Nature* 1996; **384**: 372–375.
3 Chinnaiyan AM, O'Rourke K, Yu GL *et al*. Signal transduction by DR3, a death domain-containing receptor related to TNFR-1 and CD95. *Science* 1996; **274**: 990–992.
4 Marsters SA, Sheridan JP, Donahue CJ *et al*. Apo-3, a new member of the tumor necrosis factor receptor family, contains a death domain and activates apoptosis and NF-κB. *Curr Biol* 1996; **6**: 1669–1676.
5 Shiozawa S, Hayashi S, Tsukamoto Y *et al*. Identification of the gene loci that predispose to rheumatoid arthritis. *Int Immunol* 1998; **10**: 1891–1895.
6 Shiozawa S, Hashiramoto A, Kawasaki H *et al*. Evidence for functional variation of the death receptor 3 (*DR3*) gene that inhibits apoptosis and predisposes to progressive joint destruction in 'rheumatoid arthritis. submitted for publication.
7 Grenet J, Valentine V, Kitson J, Li H, Farrow SN, Kidd VJ. Duplication of the *DR3* gene on human chromosome 1p36 and its deletion in human neuroblastoma. *Genomics* 1998; **49**: 385–393.
8 Gururajan R, Lahti JM, Grenet J *et al*. Duplication of a genomic region containing the *Cdc2L1-2* and *MMP21-22* genes on human chromosome 1p36.3 and their linkage to D1Z2. *Genome Res* 1998; **8**: 929–939.
9 Suto Y, Ishikawa Y, Hyodo H, Uchikawa M, Juji T. Gene organization and rearrangements at the human Rhesus blood group locus revealed by fiber-FISH analysis. *Hum Genet* 2000; **106**: 164–171.
10 Kemper O, Derré J, Cherif D, Engelmann H, Wallach D, Berger R. The gene for the type II (p75) tumor necrosis factor receptor (TNF-RII) is localized on band 1p36.2-p36.3. *Hum Genet* 1991; **87**: 623–624.
11 Fonatsch C, Latza U, Dürkop H, Rieder H, Stein H. Assignment of the human CD30 (Ki-1) gene to 1p36. *Genomics* 1992; **14**: 825–826.
12 Latza U, Dürkop H, Schnittger S *et al*. The human OX40 homolog: cDNA structure, expression and chromosomal assignment of the ACT35 antigen. *Eur J Immunol* 1994; **24**: 677–683.
13 Schwarz H, Arden K, Lotz M. CD137, a member of the tumor necrosis factor receptor family, is located on chromosome 1p36, in a cluster of related genes, and colocalizes with several malignancies. *Biochem Biophys Res Commun* 1997; **235**: 699–703.
14 Ohno S. *Evolution by Gene Duplication*. Springer-Verlag: Berlin, 1970.
15 Lynch M, Conery JS. The evolutionary fate and consequences of duplicate genes. *Science* 2000; **290**: 1151–1155.
16 Parra I, Windle B. High resolution visual mapping of stretched DNA by fluorescent hybridization. *Nat Genet* 1993; **5**: 17–21.
17 Fidlerová H, Senger G, Kost M, Sanseau P, Sheer D. Two simple procedures for releasing chromatin from routinely fixed cells for fluorescence *in situ* hybridization. *Cytogenet Cell Genet* 1994; **65**: 203–205.
18 Germer S, Holland MJ, Higuchi R. High-throughput SNP allele-frequency determination in pooled DNA samples by kinetic PCR. *Genome Res* 2000; **10**: 258–266.
19 Arnett FC, Edworthy SM, Bloch DA *et al*. The American rheumatism association 1987 revised criteria for the classification of rheumatoid arthritis. *Arthritis Rheum* 1988; **31**: 315–324.

Available online at www.sciencedirect.com
SCIENCE DIRECT®
Life Sciences 74 (2004) 1671–1679
Life Sciences
www.elsevier.com/locate/lifescie

Interleukin-18 induces serum amyloid A (SAA) protein production from rheumatoid synovial fibroblasts

Fumiko Tanaka[a], Kiyoshi Migita[b,*], Yojiro Kawabe[c], Takahiko Aoyagi[c], Hiroaki Ida[a], Atsushi Kawakami[a], Katsumi Eguchi[a]

[a] *First Department of Internal Medicine, Nagasaki University School of Medicine, Sakamoto1-7-1, Nagasaki, Japan*
[b] *Clinical Research Center, National Nagasaki Medical Center, Kubara 2-1001-1, Omura, Nagasaki, Japan*
[c] *Department of Rheumatology, National Ureshino Hospital, Ureshino, Saga, Japan*

Received 30 April 2003; accepted 29 August 2003

Abstract

Interleukin-18 (IL-18) is a novel proinflammatory cytokine that was recently found in synovial fluids and synovial tissues from patients with rheumatoid arthritis (RA). To investigate the role of IL-18 in rheumatoid synovitis, the levels of IL-18 and serum amyloid A (SAA) were measured in synovial fluids from 24 patients with rheumatoid arthritis (RA) and 13 patients with osteoarthritis (OA). The levels of IL-18 and SAA in the synovial fluids were elevated in RA patients. In contrast, the levels of IL-18 in synovial fluids from OA patients were significantly lower compared to those of RA patients. SAA was not detected in synovial fluids from OA patients. The expression of *SAA* mRNA in rheumatoid synovial cells was also examined. *SAA4* mRNA, which was constitutively expressed by rheumatoid synovial cells, was not affected by IL-18 stimulation. Although acute phase SAA (A-SAA, *SAA1+2*) mRNA was not detected in unstimulated synovial cells, its expression was induced by IL-18 stimulation. By immunoblot, we demonstrated that IL-18 induced the SAA protein synthesis from rheumatoid synovial cells in a dose-dependent manner. These results indicate a novel role for IL-18 in rheumatoid inflammation through the synovial SAA production.

Keywords: Amyloidosis; Interleukin-18; Rheumatoid arthritis; Serum amyloid A; Synovial cells

* Corresponding author. Clinical Research Center, National Nagasaki Medical Center, Omura, 856-8562, Japan. Fax: +81-957-54-0292.
E-mail address: migita@nmc.hosp.go.jp (K. Migita).

0024-3205/$ - see front matter © 2003 Elsevier Inc. All rights reserved.
doi:10.1016/j.lfs.2003.08.025

Introduction

The serum amyloid A (SAA) isoforms protein are precursors of amyloid A (AA) protein, a major component of the fibrous deposits in amyloidosis associated with chronic inflammatory diseases such as rheumatoid arthritis (Steel and Whitehead, 1994). SAA is an acute phase reactant synthesized by the liver in response to inflammatory cytokines and secreted in the plasma (Uhlar and Whitehead, 1999). SAA protein gene family consists of 4 members, which are divided into two classes, acute phase and constitutive SAA (Sipe, 1999). Although acute phase SAA encoded by the two genes, *SAA1* and *SAA2*, is induced by inflammatory stimuli up to 1000-fold, the constitutive *SAA4* is only inducible to a small degree (Steel et al., 1993). There is a evidence suggesting that the human *SAA3* is a pseudogene (Sellar and Whitehead, 1994). Like other acute phase proteins, SAA is synthesized in the liver, however, extrahepatic A-SAA synthesis has been confirmed, for example, in vascular smooth muscle cells and synovial cells (Meek et al., 1994; Kumon et al., 1999). Furthermore, multiple functions such as chemotaxis and collagenase induction have been assigned to SAA (Xu et al., 1995; Brinckerhoff et al., 1989). IL-18, a member of the IL-1 cytokine family, is also highly expressed in the RA synovium and is implicated in the pathogenesis of RA as a proinflammatory cytokine (Gracie et al., 1999). The present study was undertaken to assess whether IL-18 is associated with the synovial inflammation of RA. We examined the concentrations of IL-18 and SAA in synovial fluids from RA patients as well as in vitro effects of IL-18 on rheumatoid synovial cells.

Material and Methods

Patients

Patients who presented to Nagasaki University Arthritis Clinics were included in the study. Synovial fluids were obtained from 24 patients with RA diagnosed according to the 1987 revised criteria American Rheumatism Association and 13 patients with osteoarthritis (OA). Synovial fluids were removed for therapeutic purpose. The synovial fluids obtained from the study subjects were collected and stored at −20 °C.

Reagents

Recombinant human IL-18 was purchased MBL (Nagoya, Japan). The endotoxin levels were less than 0.1 ng per 1 μg of recombinant human IL-18. Human anti-SAA polyclonal antibodies were kindly provided by Dr N. Kubota (Eiken Chemicals Ltd, Tochigi, Japan)

IL-18 and SAA measurements

IL-18 and SAA were measured using specific enzyme-linked immunosorbent assay (ELISA) kits according to the manufacturer's instructions. The IL-18 ELISA kit was purchased from MBL and the SAA ELISA kit was purchased from Eiken Chemicals (Tochigi, Japan). The detection limits of the assay were as follows: 12.5 pg/ml for IL-18, 1 μg/ml for SAA.

Isolation of synovial cells

The experimental protocol was approved by the local ethics committee, and a signed informed consent was obtained from each participant prior to commencement of the study. Synovial tissue samples were obtained from patients with RA and OA during synovectomy. Synovial membranes were minced aseptically and then dissociated enzymatically with collagenase (4.0 mg/ml, Sigma) in RPMI 1640 for 4 hr at 37 °C. The obtained cells were plated on culture dishes and allowed to adhere. In order to eliminate non-adherent cells from synovial cells, the plated cells were cultured for 18 hr with RPMI 1640 supplemented with 10% fetal bovine serum (FBS) at 37 °C in humidified 5% CO_2 in air. The cells were then washed thoroughly with phosphate-buffered saline (PBS) solution. Adherent synovial cells were removed by adding trypsin-EDTA followed by washing the cells with PBS containing 2% FBS. The collected synovial cells were used at the third or fourth passages for subsequent experiments. Synovial cell preparations (fibroblast-like synovial cells) were less than 1% reactive with monoclonal antibodies CD3, CD20, and CD68 (Coulter Immunology, FL) and anti-human von Willebrand factor (Immunotech, Marseilles, France), indicating that these preparations were almost free of mature T lymphocytes, B lymphocytes, monocytes / macrophages, and vascular endothelial cells. Isolated synovial cells were cultured with RPMI 1640 media containing 10% FCS. For the experiment, medium was discarded and the cells were incubated with serum-free RPMI 1640 containing IL-18 (MBL).

RNA preparation and RT-PCR assay

RT-PCR analysis for SAA mRNA expression was performed according to the method of Kumon et al. (1999). Total cellular RNA was extracted from synovial fibroblasts using guanidium thiocyanate and phenol (RNAzol B, Cinna/Biotek Labs Int. Inc., Friendswood, TX). First-strand cDNA was synthesized by reverse transcription at 45 °C for 45 min in a 50 μl reaction mixture containing 1 μg of total RNA and MuLV reverse transcriptase (Gibco BRL, Gaithersburg, MD). After denaturing at 99 °C for 5 min followed by cooling at 5 °C, the cDNA was amplified using PCR. Two microliters of denatured cDNA was amplified a 20 μl final volume containing 1 U Taq DNA polymerase (Gibco, BRL), 1 μM of each primer, Taq polymerase buffer, 1.5 mM $MgCl_2$, and 1.5 mM of each dNTP. PCR was performed in a thermal cycler (Perkin Elmer Cetus, Foster City, CA) using a program of 31 cycles of 95 °C for 1 min, 51 °C for 1 min, and 72 °C for 1 min with a final 10 min extension at 72 °C. The amplified products were subjected to electrophoresis on 2% agarose gel.

The following specific primers were used for SAA1 + 2 (Kumon et al., 1999):

5′-CGAAGCTTCTTTTCGTTCCTT-3′ (forward), 5′-CAGGCCAGCAGGTCGGAAGTG-3′ (reverse). Predicted size of the fragment is 300 bp.
For SAA4: 5′-TTTCAAGGAGGCTCTCCAAG-3′ (forward), 5′-CCATTCCTCAGCTTTCTCGT-3′ (reverse), Predicted size of the fragment is 276 bp.
For IL-18Rα(Tanaka et al., 2001); 5′-CCCAACGATAAGAAGGAACGC-3′ (forward), 5′-TGTC-TGTGCCTCCCGTGCTGGC-3′(reverse), Predicted size of the fragment is 419 bp.
For IL-18Rβ (Tanaka et al., 2001); 5′-AACACAACCCAGTCCGTC-3′(forward), 5′-AACATCAG-GAAATAGGCTGAG-3′(reverse), Predicted size of the fragment is 291 bp.
For β-actin; 5′-GACGAGGCCCAGAGCAAGAGAG-3′ (forward), 5′-ACGTACATGGCTGGGG-TGTTG-3′(reverse), Predicted size of the fragment is 284 bp.

Immunoprecipitation and immunoblot analysis

Synovial cell-conditioned media were centrifuged at 800 g for 5 min and supernatants (0.5 ml) were pre-cleared with protein-A-Sepharose 4B (50 μl, Pharmacia, Uppsala, Sweden) for 30 min and centrifuged at 6000 g for 5 min. The pre-cleared supernatants were incubated with 5 μl of anti-SAA antibodies for 1 hr. Collection of immunocomplex was performed using protein-A Sepharose 4B (Pharmacia) for 30 min. Laemmli sample buffer (2%SDS 10% glycerol 100 mM DTT 60 mM Tris[PH6.8]) was added and boiled for 10 min. Supernatants were loaded on 14% polyacrylamide gels. The fractionated proteins were transferred to nitrocellulose membrane (pore-size: 0.2 μ, Bio-Rad, Hercules, CA) and incubated with anti-SAA antibodies (1:2000 dilution) for two hours at room temperature. The filter was rinsed and incubated with donkey anti-rabbit IgG conjugated with horseradish peroxidase (Amersham, Arlington Heights, IL) and developed using an enhanced chem-iluminesence (ECL) system (Amersham). The blots were exposed to films.

Statistical analysis

Samples with values below the detection limit for the assay were regarded as negative and assigned a value 0. The data are expressed as the mean ± standard deviations (SD) of the number patients indicated. The statistical significance of differences between 2 groups was deter-

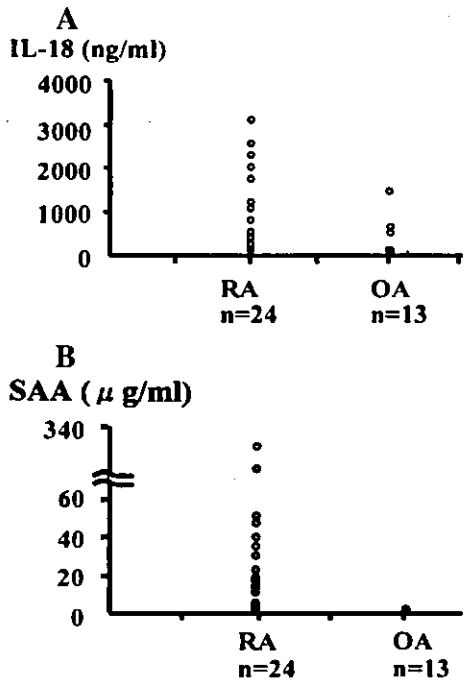

Fig. 1. Concentrations of IL-18 (A) and SAA (B) in the synovial fluid of rheumatoid arthritis (RA) and osteoarthritis (OA) patients, measured in triplicate by enzyme-linked immunosorbent assay. n = numbers of samples tested.

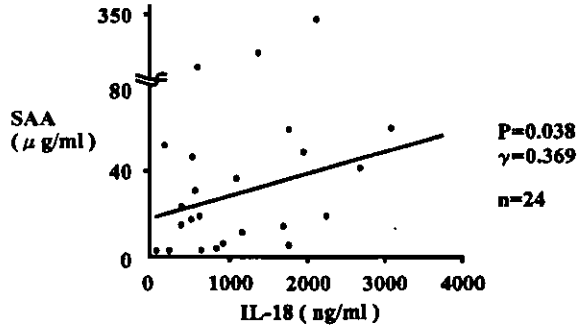

Fig. 2. Correlation between IL-18 and SAA levels in the synovial fluids of RA patients The correlation coefficient was analyzed by Peason's correlation coefficient test.

mined by Student's t-test. The correlation coefficient was obtained by Peason's correlation coefficient test.

Results

Increased IL-18 and SAA levels in the synovial fluids of RA patients

Concentrations of IL-18 in synovial fluid samples from RA and OA patients were measured by specific ELISA. As shown in Fig. 1A, the levels of IL-18 in the synovial fluids from RA patients (mean ± SD 1171.8 ± 879.5 ng/ml) were significantly higher ($p < 0.001$) than those of OA patients (mean ± SD 37.9 ± 126.6 ng/ml). We also measured the SAA concentrations of synovial fluids by means of specific ELISA using same samples. As shown in Fig. 1B, synovial SAA levels of RA patients were markedly elevated (mean ± SD 44.6 ± 68.1 μg/ml). These measurements of SAA in rheumatoid synovial fluids were similar to previous studies (Sukenik et al., 1998). On contrast, those of OA patients were below the detection limits (<2.5 μg/ml).

To investigate the relevance of IL-18 and SAA, concentrations of IL-18 were compared with those of SAA. The results suggested a possible correlation between these two values (Fig. 2). Therefore, SAA overproduction in the synovium appears to be linked to the IL-18 elevation observed in RA patients.

Fig. 3. Expression of IL-18 receptor (IL-18Rα and IL-18Rβ) mRNA in rheumatoid synovial cells. Total RNA was extracted from rheumatoid synovial cells isolated from 2 patients with RA (RA1, RAA2) and IL-18Rα and IL-18Rβ mRNA was detected by TR-PCR. Rheumatoid synovial cells constitutively expressed IL-18R mRNA.

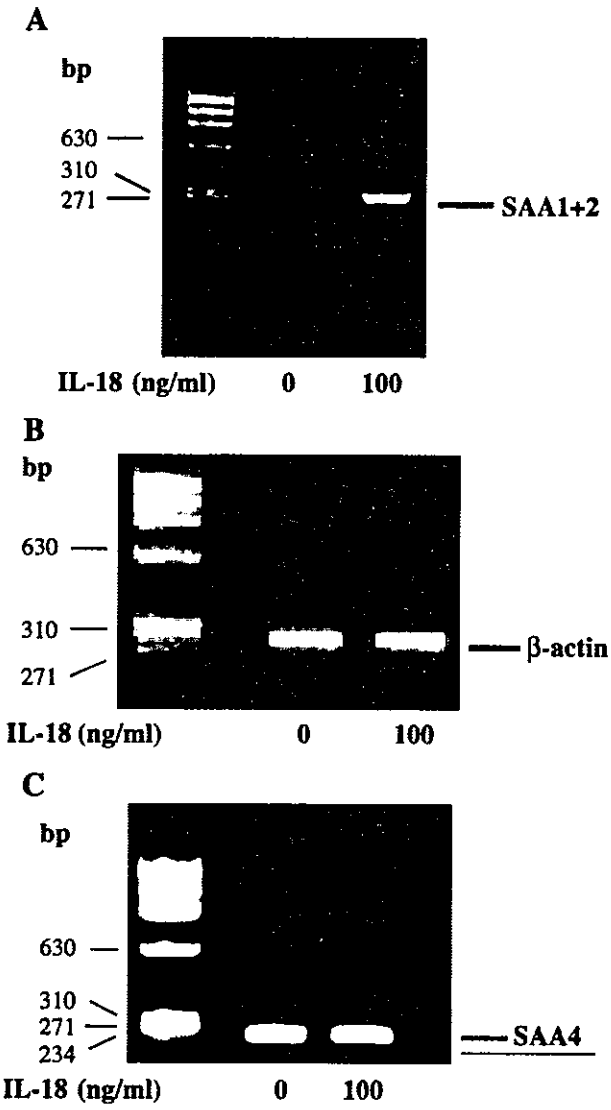

Fig. 4. A. A-SAA mRNA expression of IL-18-treated synovial cells. Rheumatoid synovial cells cultured with or without 100 ng/ml of IL-18 for 6 hr. Total RNA was extracted and amplified by RT-PCR using gene-specific primers. SAA1 + 2 mRNA was induced in IL-18-treated synovial cells. B. β-actin mRNA expression of IL-18treated synovial cells. Rheumatoid synovial cells incubated with or without 100 ng/ml of IL-18 for 6 hr. Total RNA was extracted and amplified by RT-PCR using gene-specific primers. C. C-SAA mRNA expression of IL-18treated synovial cells. Rheumatoid synovial cells incubated with or without 100 ng/ml of IL-18 for 6 hr. Total RNA was extracted and amplified by RT-PCR using gene-specific primers. The density *SAA4* mRNA bands were not different between control and IL-18-treated synovial cells. (control: 1.0 IL-18 treatment :0.93. The density of *SAA4* mRNA band was measured by densitometer. The density of *SAA4* mRNA band of untreated cells was assigned the value of 1.0 and that of IL-18-treated cells was calculated as relative units).

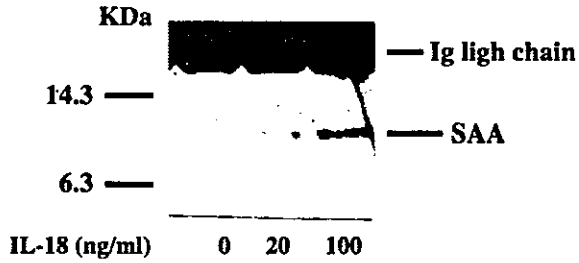

Fig. 5. SAA protein synthesis by IL-18-treated synovial cells. Rheumatoid synovial cells were cultured with IL-18 for 24 hr. The culture supernatants were removed and immunoprecipitated using ant-SAA antibodies. The immunoprecipitants were analyzed by anti-SAA immunoblot. Ig light chain indicated the light chain of immunoglubulin G that was used for immunoprecipitation.

SAA mRNA induction in IL-18-stimulated synovial cells

In order to investigate the relationship between IL-18 and SAA in rheumatoid synovium, we decided to analyze the acute phase SAA (A-SAA) mRNA expression in rheumatoid synovial cells. First, we checked the expression of IL-18 receptor in rheumatoid synovial cells. As shown in Fig. 3, IL-18Rα and IL-18Rβ mRNA were detected in rheumatoid synovial cells. SAA1 and SAA2 isoforms (A-SAA) have been identified as an acute phase reactant, and shown to be induced by proinflammatory cytokines. Next, we analyzed the *SAA1+2* mRNA expression in rheumatoid synovial cells by means of RT-PCR. As shown in Fig. 4A, *SAA1+2* mRNA was induced in IL-18-stimulated synovial cells not in unstimulated synovial cells. *SAA1+2* mRNA induction was confirmed after 6 hours of IL-18 stimulation and sustained for 24 hours (data not shown). In contrast, β-actin mRNA expression was not modulated with or without IL-18 stimulation (Fig. 4B). Constitutive-SAA (C-SAA, *SAA4*) mRNA was expressed in RA synovial cells, and were not changed by IL-18 stimulation (Fig. 4C).

SAA protein synthesis in IL-18-treated RA synovial cells

In order to further substantiate the results obtained by RT-PCR, we investigated the effects of IL-18 on de novo synthesis of SAA. We performed the immunoprecipitation of the supernatants of IL-18 treated synovial cells. RA synovial cells-conditioned media (0.5 ml) were immunoprecipitated using anti-SAA antibodies. The immunoprecipitants were fractionated by 14% polyacrylamide gels and analyzed by anti-SAA immunoblot. An immunoblot analysis of a sample of the SAA immunoprecipitates from IL-18-stimulated synovial cell-conditioned media showed an induced SAA band at 12 Kda (Fig. 5).

Discussion

IL-18 is a member of IL-1 cytokine family that was originally identified as an IFN-γ inducing factor (Akira, 2000). Similar to IL-12, IL-18 stimulates Th1 differentiation and enhances natural killer cell cytotoxicity (Dinarello, 1999). It was demonstrated that RA synovial tissues showed increased expression of IL-18 mRNA expression and increased IL-18 protein synthesis as well as IL-18 receptor